Wave Motion 130 (2024) 103386

Contents lists available at ScienceDirect

Wave Motion

journal homepage: www.elsevier.com/locate/wamot

Optical fibers with a frequency-dependent Kerr nonlinearity: Theory and applications

A.C. Sparapani [a,b,*], S.M. Hernandez [a,b], P.I. Fierens [b,c], D.F. Grosz [a,b], Govind P. Agrawal [d]

[a] Grupo de Comunicaciones Ópticas, Depto. de Ingeniería en Telecomunicaciones, Instituto Balseiro, Comisión Nacional de Energía Atómica, Río Negro 8400, Argentina

[b] Consejo Nacional de Investigaciones Científicas y Técnicas (CONICET), Ciudad Autónoma de Buenos Aires 1425, Argentina

[c] Centro de Optoelectrónica, Instituto Tecnológico de Buenos Aires (ITBA), Ciudad Autónoma de Buenos Aires 1437, Argentina

[d] The Institute of Optics, University of Rochester, Rochester, New York 14627, USA

ARTICLE INFO

Keywords:
Fiber optics
Frequency-dependent Kerr nonlinearity
Zero-nonlinearity wavelength
Photon-conserving propagation
Optical switching

ABSTRACT

This review provides a detailed discussion of both the mathematical treatment and the impact of a frequency-dependent Kerr nonlinearity on the propagation of short pulses in optical fibers. We revisit the theoretical framework required to deal with the frequency dependence of the nonlinear response without incurring any physical inconsistencies, such as the non-conservation of the photon number. Then, we point out the role of the zero-nonlinearity wavelength, its interplay with the zero-dispersion wavelength, and their influence on evolution of optical pulses in optical fibers, specifically by looking at soliton propagation and the ensuing generation of Cherenkov radiation. Finally, by means of a space–time analogy involving the collision of a weak control pulse and an intense soliton, we describe an all-optical switching scheme in the presence of a zero-nonlinearity wavelength within a photon-conserving framework.

1. Introduction

The advent of optical fibers has had a profound impact on modern science and technology. An example is provided by the telecommunication revolution, spurred by the introduction of low-loss optical fibers in the 1970s [1] and the development of erbium-doped fiber amplifiers in the late 1980s [2–5]. The unique feature of optical fibers is that they exhibit an extremely low loss in the near-infrared region near 1550 nm. This feature, together with a strong field confinement, leads to long interaction lengths compared to bulk media and makes optical fibers an ideal platform for the generation and study of several nonlinear optical effects. While such effects are mostly detrimental in the realm of optical communication (see Ref. [6] for a review), they are used advantageously for a vast number of photonic applications, ranging from optical sensors [7–19], tunable laser sources [20–33], to optical frequency combs, which have revolutionized the search of exoplanets in recent years [34].

The prediction of the existence of solitons in optical fibers around 1973 [35,36], and their experimental observation in the year 1980 [37], opened up a new research area with a wide range applications. Solitons are short pulses that are able to propagate long distances unperturbed due to a balance between the dispersive (linear) and nonlinear effects, the latter caused by the dependence of the fiber's refraction index on the local intensity, a phenomenon known as the optical Kerr effect. The introduction of photonic crystal fibers (PCFs) in the 1990s [38–51] fueled further interest in nonlinear fiber optics. PCFs allow for the engineering of

* Corresponding author at: Grupo de Comunicaciones Ópticas, Depto. de Ingeniería en Telecomunicaciones, Instituto Balseiro, Comisión Nacional de Energía Atómica, Río Negro 8400, Argentina.

E-mail address: alexis.sparapani@ib.edu.ar (A.C. Sparapani).

https://doi.org/10.1016/j.wavemoti.2024.103386
Received 14 May 2024; Received in revised form 19 June 2024; Accepted 2 July 2024
Available online 8 July 2024

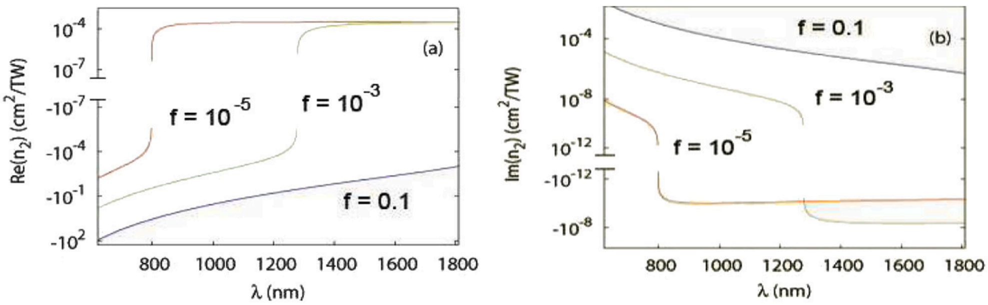

Fig. 1. Wavelength dependence of the real (left) and imaginary (right) parts of the nonlinear coefficient n_2 for several filling factors f in a silica glass doped with silver nanoparticles.
Source: Reproduced with permission from Ref. [78].

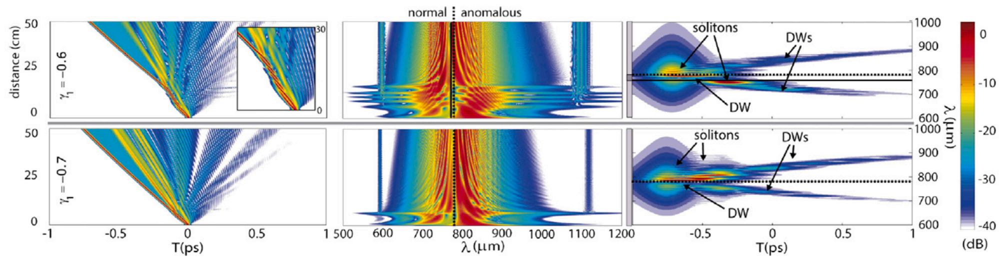

Fig. 2. Evolution of a fundamental soliton in a PCF for two different frequency-dependent nonlinear profiles, portraying how this dependence leads to substantially different outcomes. DWs: dispersive waves. For reference, values of the first-order nonlinear parameter are $\gamma_1 = -0.6$ (top) and $\gamma_1 = -0.7\,\mathrm{fs}\ /\ (\mathrm{w\,m})$ (bottom) (see Section 2.6).
Source: Reproduced with permission from Ref. [79].

desired dispersion profiles while providing an enhanced confinement of the optical field, a feature favoring the onset of nonlinear phenomena. A paradigmatic example of the PCF advantage is provided by the supercontinuum generation, *i.e.*, intense coherent broadband light, first observed by Ranka et al. [42]. Since then, supercontinuum sources have found applications in such diverse areas as spectroscopy [52–64], microscopy [65–68], optical coherence tomography [69–74], and metrology [75,76].

In scenarios such as supercontinuum generation and others involving propagation of ultrashort pulses inside optical fibers, the spectral range of interest becomes so wide that the consideration of the frequency dependence of the fiber's nonlinear parameter becomes paramount. As early as 2005, this was made clear in the work of Kibler et al. [77], where the dependence of the PCF's effective area (see Fig. 1 in Ref. [77]), introduced through the so-called shock term in the generalized nonlinear Schrödinger equation [6], was shown to lead to a reduction in the Raman-induced frequency shift of the soliton on the red edge of the broadband spectrum.

Most interestingly, it was found that frequency dependence of the nonlinear response of optical fibers can be modified with the inclusion of metal nanoparticles inside their core. Such an approach was pursued in 2009 by Driben et al., who studied the generation of low-threshold supercontinuum [78] and propagation of solitons [80] in silica glasses doped with silver nanoparticles. Using a Maxwell–Garnet model, the composite medium was shown to exhibit a highly frequency-dependent Kerr parameter, which could even acquire negative values depending on the filling factor of nanoparticles, as shown in Fig. 1. Recently, solitary wave propagation was shown to be possible over several soliton periods in the normal dispersion regime of silica glasses doped with silver nanoparticles [81].

When the core of an optical fiber is doped with metal nanoparticles, its nonlinear parameter γ not only varies with frequency but may also vanish at a specific wavelength known as the zero-nonlinearity wavelength (ZNW). Such fibers often exhibit a zero-dispersion wavelength (ZDW), in addition to the ZNW, at which the second-order dispersion parameter β_2 vanishes. Solitons require a positive γ but anomalous dispersion such that β_2 has a negative value. It should be clear that this combinations can occur in only specific spectral regions. Bose et al. [82–86] have studied numerically the dynamics of fundamental and higher-order solitons inside PCFs exhibiting a frequency-dependent Kerr nonlinearity, with emphasis on the relative positions of the ZNW and ZDW. In particular, they identified tunneling of a fundamental soliton from one solitonic spectral band to another through an intervening non-solitonic region.

In the work of Arteaga-Sierra et al. [79] (see also Refs. [87,88]), the soliton self-frequency shift (SSFS) was shown to be either enhanced or suppressed in PCFs with a frequency-dependent Kerr nonlinearity, depending on the sign of the slope of the nonlinear parameter as a function of frequency. Moreover, this suppression of the SSFS was shown to occur without a spectral recoil and energy transfer to a dispersive wave (see Fig. 2). In a recent work, Melchert et al. [89] considered optical waveguides with a ZNW and found that solitons can form in the normal-dispersion regime when γ is negative. They also studied two-color compound pulses and found that they can endure higher-order dispersion, self-steepening, and Raman scattering better than a single pulse.

When tackling the problem of propagation of short pulses in optical fibers with a frequency-dependent Kerr nonlinearity, care must be taken to ensure that the nonlinear Schrödinger equation (NLSE) and its generalized version (GNLSE) do not produce unphysical results. This is particularly relevant when the GNLSE includes effects of self-steepening [6,77,90–92] and intrapulse Raman scattering [6,93–97]. As it was recognized in the work of Blow and Wood [90], the NLSE fails to preserve the number of photons, even in a lossless medium, unless dependence of the nonlinear parameter on frequency is assumed to be of the form $\tilde{\gamma}(\omega) = \gamma_0 + \gamma_1(\omega - \omega_0)$, and the slope set to $\gamma_1 = \gamma_0/\omega_0$, where γ_0 is the nonlinear parameter evaluated at the central frequency ω_0.

In the case of PCFs with an arbitrary frequency-dependent nonlinear profile, one must resort to propagation equations that strictly ensure the conservation of the number of photons. Recently, Bonetti et al. introduced the photon-conserving NLSE (pcNLSE) [98] and its generalized version (pcGNLSE) [99]. These propagation equations were subsequently used to revisit soliton dynamics in optical waveguides by Linale et al. [100]. The same authors also put forth a novel method to obtain the slope of the nonlinear parameter [101], whose value can depart significantly from the usually adopted form of $\gamma_1 = \gamma_0/\omega_0$, by measuring the delay experienced by a soliton with respect to a low-amplitude reference pulse. Further, soliton solutions of the pcNLSE and a derivation of that delay and its relation to the medium self-steepening parameter were studied by Hernandez et al. [102]. Interestingly, a linear stability analysis of the pcNLSE leads to a richer and more complex scenario of the phenomenon of modulation instability, compared to the well-known results obtained with the NLSE [103]. Such an analysis emphasizes the role of the ZNW in a more clear fashion in such systems. Results obtained with the pcNLSE that depart from those of the NLSE are discussed further in Section 2.6.

The influence of a frequency-dependent nonlinearity has also been recognized in the area of integrated photonics, specifically in the propagation of short pulses in silicon nanowires decorated with a two-dimensional (2D) material such as graphene, whose addition can generate a supercontinuum over short distances at relatively low pump powers [104–108]. The presence of a 2D medium not only enhances the nonlinear response of the nanowire but also its dependence on frequency. As discussed earlier, numerical modeling of such nanowires must be approached with care to correctly account for the evolution of the photon number.

In this work, we review results on the propagation in optical fibers with a frequency-dependent nonlinearity. Section 2 presents the derivation of several propagation equations that account for such frequency dependence, pointing out advantages and disadvantages of each of them. Section 3 discusses the interesting case where the nonlinearity changes sign in the spectral region under consideration. Finally, Section 4 closes this paper with some final remarks and conclusions.

2. Propagation under a frequency-dependent nonlinearity

In this section, we review several propagation equations used for studying nonlinear phenomena in optical waveguides. Section 2.1 shows the derivation of a first-order differential equation from the well-known Maxwell's equations in the frequency domain. The widely used nonlinear Schrödinger equation is presented in Section 2.2, where we also highlight the approximations needed to derive it. Section 2.4 explains how a simple frequency dependence of the nonlinearity is incorporated in a generalized nonlinear Schrödinger equation. Other approaches used for handling the frequency dependence of the nonlinearity are summarized in Section 2.5. Finally, we introduce the photon-conserving generalized nonlinear Schrödinger equation in Section 2.6.

2.1. Preliminaries

As usual, we employ Maxwell's equations to arrive at the following wave equation for the electric field [6,97,109]

$$\nabla^2 \mathbf{E}(\mathbf{r},t) - \mu_0\epsilon_0 \frac{\partial^2 \mathbf{E}(\mathbf{r},t)}{\partial t^2} = -\mu_0 \frac{\partial^2 \mathbf{P}(\mathbf{r},t)}{\partial t^2}, \tag{1}$$

where $\mathbf{r} = (x, y, z)$ is the coordinate vector, $\mathbf{E}$ is the electric field vector, $\mathbf{H}$ the magnetic field, $\mathbf{P}$ is the induced polarization vector, ϵ_0 is the vacuum permittivity and μ_0 is the vacuum permeability. This equation is valid for nonmagnetic materials and makes use of the approximation $\nabla \cdot \mathbf{E} \approx 0$, which holds well in many cases [97,110], although it is not exact even in the case of an isotropic medium [111]. The polarization vector can be split into two parts, depending on whether its dependence on the electric field is linear or nonlinear: $\mathbf{P} = \mathbf{P}^{\mathrm{L}} + \mathbf{P}^{\mathrm{NL}}$. In a centrosymmetric material, these two parts take following form in the electric-dipole approximation and assuming a local response [97,109]:

$$\mathbf{P}^{\mathrm{L}}(\mathbf{r},t) = \epsilon_0 \int_{-\infty}^{t} dt_1 \chi^{(1)}(\mathbf{r}, t-t_1) \cdot \mathbf{E}(\mathbf{r}, t_1), \tag{2}$$

$$\mathbf{P}^{\mathrm{NL}}(\mathbf{r},t) = \epsilon_0 \int_{-\infty}^{t} dt_1 \int_{-\infty}^{t} dt_2 \int_{-\infty}^{t} dt_3 \, \chi^{(3)}(\mathbf{r}, t-t_1, t-t_2, t-t_3) \,\vdots\, \mathbf{E}(\mathbf{r},t_1)\mathbf{E}(\mathbf{r},t_2)\mathbf{E}(\mathbf{r},t_3), \tag{3}$$

where the symbol $\vdots$ denotes a tensor product, $\chi^{(1)}$ and $\chi^{(3)}$ are the first-order and third-order susceptibilities, respectively. As usual, we have neglected higher order nonlinear terms.

For the sake of simplicity, let us assume that the susceptibilities do not depend on the propagation direction, assumed to coincide with the z axis. Then, Eq. (1) can be written in the frequency domain as

$$\left\{ \frac{\partial^2}{\partial z^2} + \nabla_\perp^2 + \left[\frac{\omega \mathrm{n}(\mathbf{r}_\perp, \omega)}{c} \right]^2 \right\} \tilde{\mathbf{E}}(\mathbf{r},\omega) = -\left[\frac{\omega}{c}\right]^2 \tilde{\mathbf{Q}}^{\mathrm{NL}}(\mathbf{r},\omega), \tag{4}$$

where we have defined the Fourier transform as $\mathcal{F}\{\cdot\} = \int_{\mathbb{R}} \cdot \exp\{i\omega t\}dt$, the refractive index $\mathrm{n}^2(\mathbf{r}_\perp,\omega) = 1 + \tilde{\chi}^{(1)}(\mathbf{r}_\perp,\omega)$, $\tilde{\mathbf{Q}}^{\mathrm{NL}}(\mathbf{r},\omega) = \epsilon_0^{-1}\tilde{\mathbf{P}}^{\mathrm{NL}}(\mathbf{r},\omega)$, c is the speed of light in vacuum, and $\nabla_\perp^2$ is the Laplacian operator with respect to $\mathbf{r}_\perp = (x,y)$. Following the development in Ferrando et al. [110], let us define the operator $\mathcal{L} = \nabla_\perp^2 + (\omega\mathrm{n}(\mathbf{r}_\perp,\omega)/c)^2$ and consider the eigenvalue equation

$$\mathcal{L}\tilde{\mathbf{F}}_n(\mathbf{r}_\perp,\omega) = \tilde{\beta}_n^2(\omega)\tilde{\mathbf{F}}_n(\mathbf{r}_\perp,\omega). \tag{5}$$

Given that $\mathcal{L}$ does not mix the electric field polarizations, the eigenmodes $\tilde{\mathbf{F}}_n$ are three-fold degenerate. Let $\{\mathbf{u}_1,\mathbf{u}_2,\mathbf{u}_3\}$ be an orthonormal basis for the polarization modes and let us define $\tilde{\mathbf{F}}_{n,i} = \tilde{F}_n\mathbf{u}_i$ where $\tilde{F}_n$ is an eigenfunction of Eq. (5) with eigenvalue $\tilde{\beta}_n^2$. In a lossless medium (real-valued n), $\mathcal{L}$ is self-adjoint and, hence, $\{\tilde{\mathbf{F}}_{n,i}\}_{n,i}$ forms an orthogonal basis of functions that enables us to expand the electric field as

$$\tilde{\mathbf{E}}(\mathbf{r},\omega) = \sum_{n,i}\tilde{A}_{n,i}(z,\omega)\tilde{\mathbf{F}}_{n,i}. \tag{6}$$

If we further assume, without loss of generality, that modes $\tilde{F}_n$ are normalized, then Eqs. (4) and (6) can be combined to obtain

$$\left(\frac{\partial^2}{\partial z^2} + \tilde{\beta}_n^2(\omega)\right)\tilde{A}_{n,i}(z,\omega) = -\left(\frac{\omega}{c}\right)^2\tilde{Q}_{n,i}^{\mathrm{NL}}(z,\omega). \tag{7}$$

It can be shown that $\tilde{A}_{n,i}(z,\omega) = \tilde{A}_{n,i}^F(z,\omega) + \tilde{A}_{n,i}^B(z,\omega)$ such that

$$\left(-\mathrm{i}\frac{\partial}{\partial z} - \tilde{\beta}_n(\omega)\right)\tilde{A}_{n,i}^F(z,\omega) = +\frac{1}{2\tilde{\beta}_n(\omega)}\left(\frac{\omega}{c}\right)^2\tilde{Q}_{n,i}^{\mathrm{NL}}(\mathbf{r},\omega), \tag{8}$$

$$\left(-\mathrm{i}\frac{\partial}{\partial z} + \tilde{\beta}_n(\omega)\right)\tilde{A}_{n,i}^B(z,\omega) = -\frac{1}{2\tilde{\beta}_n(\omega)}\left(\frac{\omega}{c}\right)^2\tilde{Q}_{n,i}^{\mathrm{NL}}(\mathbf{r},\omega). \tag{9}$$

Eqs. (8) and (9) describe two waves, one traveling forward and another backward. Observe, however, that these two equations are coupled through the terms on the right side involving a nonlinear interaction between $\tilde{A}_{n,i}^F$ and $\tilde{A}_{n,i}^B$.

All in all, we have arrived at two couple first-order propagation equations, one for a forward and another for a backward propagating wave. In order to neglect the backward propagating equation, several arguments have been put forth in the literature, such as the *slowly-varying-envelope* approximation [6,109], the *slowly-evolving-wave approximation* [112], the *slowly-evolving envelope approximation* [113], the *generalized few-cycle envelope approximation* [114,115], and some other linearization approaches [116,117]. Other authors have straightforwardly neglected the backward propagation [90,92,109,111,118–120]. Further studies on the validity of the forward-only approximation can be found in Refs. [121–129]. In what follows, we neglect the interaction of the forward and backward propagating waves. We must note that these equations were derived for the lossless case, but they can be generalized to nonlinear media with a complex-valued refractive index.

For the sake of clarity, we shall assume that there is a single mode propagating in the waveguide and the field is linearly polarized. The discussion that follows can be extended to the more general multimode vectorial case, but equations become quite cumbersome and do not shed more light into the subject at hand. With these simplifications, the forward propagation equations can be written as

$$\left(-\mathrm{i}\frac{\partial}{\partial z} - \tilde{\beta}(\omega)\right)\tilde{A}(z,\omega) = +\frac{1}{2\tilde{\beta}(\omega)}\left(\frac{\omega}{c}\right)^2\tilde{Q}^{\mathrm{NL}}(z,\omega), \tag{10}$$

$$\begin{aligned}\tilde{Q}^{\mathrm{NL}}(z,\omega) = &\iint_{\mathbb{R}^2} d\omega_1 d\omega_2 \tilde{A}^*(z,\omega_1)\tilde{A}(z,\omega_2)\tilde{A}(z,\omega+\omega_1-\omega_2)\\ &\times R(\omega,\omega_1,\omega_2,\omega+\omega_1-\omega_2),\end{aligned} \tag{11}$$

$$\begin{aligned}&R(\omega,\omega_1,\omega_2,\omega+\omega_1-\omega_2) =\\ &\quad 3\iint_{\mathbb{R}^2} dxdy\tilde{\chi}^{(3)}(x,y,\omega,\omega_1,\omega_2,\omega+\omega_1-\omega_2)\\ &\quad\times \tilde{F}^*(x,y,\omega)\tilde{F}^*(x,y,\omega_1)\tilde{F}(x,y,\omega_2)\tilde{F}(x,y,\omega+\omega_1-\omega_2),\end{aligned} \tag{12}$$

where the factor 3 comes from the three-fold degeneracy. As can be observed from Eq. (12), in general, frequency dependence of the nonlinear term is far from being simple. In the remaining of this section, we shall present different strategies for dealing with this complexity.

2.2. Nonlinear Schrödinger equation

One simplification assumes that the nonlinear response is instantaneous, that is, $\chi^{(3)}(\mathbf{r},t_1,t_2,t_3) = \overline{\chi}^{(3)}(\mathbf{r})\delta(t_1)\delta(t_2)\delta(t_3)$. As stated in Ref. [6], this assumption amounts to neglecting the contributions of molecular vibrations (*e.g.*, the Raman effect) to the nonlinearity as they occur on a longer time-scale ($\sim$ 60 fs for silica optical fibers). We must note that this assumption implicitly presupposes that there is no dependence of the third order susceptibility on frequency. Even so, the nonlinearity may vary with the wavelength through the mode-shape dispersion. If we further assume that the transversal mode shape does not change much with frequency and set $\tilde{F}(x,y,\omega) \approx F(x,y)$, we have

$$\tilde{Q}^{\mathrm{NL}}(z,\omega) = R_0\,\mathcal{F}\{A(z,t)|A(z,t)|^2\}_\omega, \tag{13}$$

$$R_0 = 3 \iint_{\mathbb{R}^2} dx\,dy\, \overline{\chi}^{(3)}(x,y)\, |F(x,y)|^4\,. \tag{14}$$

Eq. (14) can be further simplified if we assume that the susceptibility does not the depend on the transverse coordinates, but we do not need to do so here.

Observe that even with all these simplifications, the right-hand side of Eq. (10) still depends on the frequency. In order to eliminate such dependence, we need to further approximate

$$\frac{1}{2\tilde{\beta}(\omega)}\left(\frac{\omega}{c}\right)^2 \approx \frac{1}{2\tilde{\beta}(\omega_0)}\left(\frac{\omega_0}{c}\right)^2, \tag{15}$$

for an adequately chosen "central" frequency ω_0. Let us write $\beta_0 = \tilde{\beta}(\omega_0)$, $A(z,t) = G(z,t)e^{i\omega_0 t - i\beta_0 z}$, $\Omega = \omega - \omega_0$ and $\tilde{\beta}(\Omega) = \sum_{k=0}^{\infty} \beta_k \Omega^k/k!$. Then, the propagation equation in time domain becomes

$$\frac{\partial G(z,t)}{\partial z} = \mathrm{i}\sum_{k=1}^{\infty} \frac{\mathrm{i}^k \beta_k}{k!}\frac{\partial^k G(z,t)}{\partial t^k} + \mathrm{i}\gamma_0\, G(z,t)|G(z,t)|^2, \tag{16}$$

with $\gamma_0 = R_0\omega_0^2/2\beta_0 c^2$. If we limit the Taylor series up to the second term, this expression is reduced to the form of the well-known nonlinear Schrödinger equation (NLSE). Eq. (16) is also used in the field of matter waves for analyzing atomic Bose–Einstein condensates (BEC), and is often called the Gross–Pitaevskii equation (GPE) [130]. In that case, a scalar potential appears on the right side of Eq. (16), which is also present when modeling the propagation of optical pulses in some particular settings (see, *e.g.*, [131–134]).

Let us define the quantities

$$\sigma(z) = \int_{\mathbb{R}} |\tilde{G}(z,\Omega)|^2 d\Omega, \qquad \Phi(z) = \int_{\mathbb{R}} \frac{|\tilde{G}(z,\Omega)|^2}{\Omega + \omega_0} d\Omega, \tag{17}$$

which are proportional to the energy and the photon number, respectively. If we assume negligible losses in the waveguide, *i.e.*, β_k and R_0, are real quantities, it can be shown using Eq. (16) that $\partial\sigma/\partial z = 0$, and $\partial\Phi/\partial z \neq 0$. Thus, the propagation equation with a frequency independent nonlinearity conserves energy, but it does not conserve the photon number. This unphysical result, already noticed by Blow and Wood [90], discredits the approximations made to arrive at Eq. (16). Nonetheless, the NLSE is amply used and its predictions have been verified in a wide variety of cases. It also allows us make a crude estimation of the order of magnitude of the error caused by neglecting the backward-propagating wave, as we show in what follows.

2.3. Order of magnitude of the backward-propagating wave

Let us assume a narrowband setting such that the approximations that lead to Eq. (16) are valid. Then, it can be shown, departing from Eqs. (8)–(9), that

$$\left|\frac{A^B(z,t)}{A^F(z,t)}\right|^2 \sim 4\left(\frac{\gamma_0 P_0}{\gamma_0 P_0 + 2\beta_0}\right)^2. \tag{18}$$

where P_0 is the initial peak power of the forward-propagating wave. For the sake of simplicity, we have assumed that $\beta_k = 0$ for $k > 0$ and $|A^F| \gg |A^B|$.

In a standard communications fiber, $\gamma_0 \approx 0.01\,\mathrm{W}^{-1}\mathrm{m}^{-1}$. For a silica waveguide at 1500 nm, $\beta_0 \approx 6\times 10^6\mathrm{m}^{-1}$ (see Chapter 1 of Ref. [6]). If $P_0 = 10\,\mathrm{W}$, then $|A^B(z,t)/A^F(z,t)|^2 \sim 3\times 10^{-14}$. If, on the contrary, we assume a large nonlinearity $\gamma_0 = 1\,\mathrm{W}^{-1}\mathrm{m}^{-1}$ (see, *e.g.*, Chapter 11 of Ref. [6]) and a large power $P_0 = 1\,\mathrm{MW}$, $|A^B(z,t)/A^F(z,t)|^2 \sim 0.02$. Thus, neglect of the backward-propagating wave seems to be reasonable, even for very large nonlinearities and input powers, even though in these cases the effect might be noticeable. Furthermore, we shall show that the problems in photon-number conservation of the NLSE (or its simple extension to a frequency-dependent nonlinearity in the following section) are far more serious than error caused by neglecting the backward-propagating wave.

2.4. Simple frequency dependence of the nonlinearity

A simple approach to recover the frequency dependence of the nonlinearity is to merely replace γ_0 in Eq. (16) by a function $\tilde{\gamma}(\Omega)$. Writing the Taylor expansion of $\tilde{\gamma}$ as $\tilde{\gamma}(\Omega) = \sum_{k=0}^{\infty}\gamma_k\Omega^k/k!$, we arrive at

$$\frac{\partial G(z,t)}{\partial z} = \mathrm{i}\sum_{k=1}^{\infty} \frac{\mathrm{i}^k \beta_k}{k!}\frac{\partial^k G(z,t)}{\partial t^k} + \mathrm{i}\left(\sum_{k=0}^{\infty}\frac{\mathrm{i}^k\gamma_k}{k!}\frac{\partial^k}{\partial t^k}\right) G(z,t)|G(z,t)|^2. \tag{19}$$

In this sense, Eq. (16) can be considered a narrowband approximation of Eq. (19). Furthermore, it is often found sufficient to include only the first two terms in the Taylor expansion. The term with γ_1 is known to be responsible for the self-steepening phenomenon [6,77,90–92].

However, in view of Eqs. (10)–(12), it is not clear whether such an *ad hoc* addition of frequency dependence to the nonlinearity is well justified. One justification found in the literature, appeals to the work of Hellwarth [135]. The author argues that the Born–Oppenheimer approximation is valid for the expected nonlinear polarization in transparent non-conducting media whose electronic gap-frequency is much higher than the optical frequencies (for example, mid-infrared frequencies in silica fibers). By only focusing on optical frequencies well above the nuclear-response frequencies, Hellwarth shows that

$$\chi^{(3)}(\mathbf{r},t_1,t_2,t_3) = \overline{\chi}^{(3)}(\mathbf{r})\delta(t_1)\delta(t_2)\delta(t_3) + \delta(t_1)\hat{\chi}^{(3)}(\mathbf{r},t_1-t_2)\delta(t_2-t_3), \tag{20}$$

where $\overline{\chi}^{(3)}$ corresponds to the electronic response and $\hat{\chi}^{(3)}$ describes nuclear nonlinearities, such as the Raman effect. Tang and Sutherland [136] (see also Ref. [137]) depart from Hellwarth [135], but they do not delve into the details of the mathematical derivation. In turn, they consider two types of nonlinearities, instantaneous and with an exponential decay. The first type is clearly represented by the first term in the last equation. For the other type of nonlinearity, they argue intuitively based on a scheme where two coincident optical fields cause a distortion in the medium and, and a third field arriving during the exponential decay produces the nonlinear response. This reasoning leads them to a (time) symmetrized version of the second term in Eq. (20), which after some manipulations takes the form

$$\begin{aligned} R(\omega,\omega_1,\omega_2,\omega+\omega_1-\omega_3) = 3 \iint_{\mathbb{R}^2} dx\,dy\, \tilde{\chi}^{(3)}(x,y,\omega) \\ \times \tilde{F}^*(x,y,\omega)\tilde{F}^*(x,y,\omega_1)\tilde{F}(x,y,\omega_2)\tilde{F}(x,y,\omega+\omega_1-\omega_2), \end{aligned} \tag{21}$$

where, for the sake of simplicity, we wrote $\tilde{\chi}^{(3)}(\mathbf{r},\omega,\omega_1,\omega_2,\omega+\omega_1-\omega_2) = \tilde{\chi}^{(3)}(\mathbf{r},\omega)$. Thus, using the approach of Hellwarth [135], or that of Tang and Sutherland [136], does not reduce complexity of the frequency dependence of the nonlinearity. A further assumption is needed, for example, that the mode shape does not change too much over frequencies of interest, i.e.,

$$\tilde{F}(x,y,\omega_1) \approx \tilde{F}(x,y,\omega_2) \approx \tilde{F}(x,y,\omega+\omega_1-\omega_2) \approx \tilde{F}(x,y,\omega). \tag{22}$$

Armed with this new assumption, we can finally write

$$R(\omega) = 3\tilde{\chi}^{(3)}(\omega) \iint_{\mathbb{R}^2} dx\,dy\, \left|\tilde{F}(x,y,\omega)\right|^4 = \frac{3\tilde{\chi}^{(3)}(\omega)}{\mathrm{A_{eff}}(\omega)}, \tag{23}$$

where $\mathrm{A_{eff}}$ is the effective mode area and, for the sake of simplicity, we assumed that $\tilde{\chi}^{(3)}$ does not depend on $\mathbf{r}_\perp$. We can also think of a waveguide that is homogeneous or a sort of "effective" third order susceptibility which can be factored out of the integral.

Let us define

$$\tilde{K}(z,\omega) = \sqrt{\frac{c\epsilon_0 \mathrm{n}(\omega)}{2}}\tilde{G}(z,\omega), \tag{24}$$

so that $|K(z,t)|^2$ is the optical power if $\mathrm{n}(\omega)$ does not change much with frequency, which is usually a good assumption [77]. Furthermore, it is customary to define the effective refractive index and the effective nonlinear refraction as

$$\mathrm{n_{eff}}(\Omega) = \frac{\tilde{\beta}(\Omega)}{(\Omega+\omega_0)c}, \qquad \mathrm{n}_2 = \frac{3\overline{\chi}^{(3)}}{c\epsilon_0|n|}, \tag{25}$$

respectively. Let us note that we have defined n_2 in such a way that it is frequency independent, which is a good approximation for many materials [77]. Furthermore, it has been shown to have a negligible frequency dependence far from ultraviolet resonances in fused silica [138]. Given these definitions, we can rewrite the propagation equation in the frequency domain as (see Chapter 2 of Agrawal [6])

$$\frac{\partial \tilde{K}(z,\Omega)}{\partial z} = i\tilde{\beta}'(\Omega)\tilde{K}(z,\Omega) + i\tilde{\gamma}'(\Omega)\tilde{Q}^{\mathrm{NL}''}(z,\Omega), \tag{26}$$

$$Q^{\mathrm{NL}''}(z,t) = K(z,t)\int_{\mathbb{R}} dt_1\, h(t-t_1)|K(z,t_1)|^2, \tag{27}$$

$$\tilde{\gamma}'(\Omega) = \frac{(\Omega+\omega_0)\,\mathrm{n}_2}{\mathrm{n_{eff}}(\Omega)\mathrm{A_{eff}}(\Omega)c}. \tag{28}$$

with $\tilde{h}(\omega) = 1 + \tilde{\chi}^{(3)}(\omega)/\overline{\chi}^{(3)}$, and $\tilde{\beta}' = \tilde{\beta} - \beta_0$. This equation is known as the generalized nonlinear Schrödinger equation (GNLSE) and, with some minor modifications, have been put forth in Refs. [90–92] (see, also, Chapter 2 of Agrawal [6]). To a first order in Ω, the nonlinear parameter $\tilde{\gamma}'$ can be written as [77,90,92]

$$\tilde{\gamma}'(\Omega) = \tilde{\gamma}'(0)\,\left(1+\tau_s\Omega\right) \tag{29}$$

$$\tau_s = \frac{1}{\omega_0} - \frac{\partial}{\partial z}\ln\left(\mathrm{n_{eff}}(\Omega)\mathrm{A_{eff}}(\Omega)\right)\Big|_{\Omega=0}. \tag{30}$$

τ_s is a value associated to the effect of self-steepening and optical shock formation.

It is interesting to note that Eq. (26) is the generalized Gross–Pitaevskii equation used to model the nonlocal boson interactions. Indeed, by interchanging space and time variables, the function $h(t)$ represents the nonlocal kernel (see, *e.g.*, García-Ripoll et al. [139]). This connection between the models of a weak spatial nonlocality in Bose–Einstein condensates and the frequency dependence of nonlinearity in fiber optics deserves further study as results in one field may shed light on the other.

In the absence of losses and given Raman scattering is included, the number of photons should be conserved, but not energy. In the lossless case, $\tilde{\beta}'$, n_2 and $\mathrm{A_{eff}}$ are real-valued functions. Under this assumption, Blow and Wood [90] showed that the conserved quantity is

$$\Psi(z) = \int_{\mathbb{R}} d\Omega\, \mathrm{n}_{\mathrm{eff}}(\Omega)\mathrm{A}_{\mathrm{eff}}(\Omega)\frac{|\tilde{K}(z,\Omega)|^2}{\Omega+\omega_0}. \tag{31}$$

$\Psi(z)$ is proportional to the number of photons if and only if $\mathrm{n}_{\mathrm{eff}}$ and $\mathrm{A}_{\mathrm{eff}}$ do not depend on frequency. In view of Eq. (30), this implies that $\tau_s = \omega_0^{-1}$. However, this is not the case in general [77]. For example, Panoiu et al. [140,141] found that τ_s can be even negative in silicon photonic wires at frequencies far from ω_0. Thus, the GNLSE (Eq. (26)) does not conserve the photon number in general.

2.5. Other approaches

Lægsgaard [142] payed special attention to the problem of photon conservation, taking into account modal dispersion. Without getting into the details (the interested reader is referred to Refs. [143–145]), we can mention that the author follows the development in Kolesik et al. [146] where a propagation equation is derived on the basis of a decomposition in eigenmodes, but without normalization. The resulting equation is proved to conserve the photon number, but it cannot be numerically solved with a similar efficiency as Eq. (26). Thus, the author appeals to an interesting factorization of the nonlinear coefficient which leads to an equation similar to the GNLSE that conserves the photon number in a lossless waveguide. That factorization is akin to turning Eq. (12) into

$$R(\omega,\omega_1,\omega_2,\omega+\omega_1-\omega_2) \propto \tilde{\phi}^*(\omega)\tilde{\phi}^*(\omega_1)\tilde{\phi}(\omega_2)\tilde{\phi}(\omega+\omega_1-\omega_2). \tag{32}$$

This type of factorization is also found in all other photon-conserving approaches.

A very different approach is followed by Amiranashvili and Demircan [125] (see also Refs. [126,128,129]). The authors start from Maxwell's equations for linearly polarized fields and use a Fourier series to write the electric field as

$$E(z,t) = \sum_{k\in\mathbb{Z}} \tilde{E}(z,\omega_k)e^{-\mathrm{i}\omega_k t}, \qquad \omega_k = \frac{2\pi\, k}{T}, \tag{33}$$

for some period T. They introduce a complex electric field $\tilde{A}(z,\omega_k)$ such that $E(z,t) = \mathrm{Re}\{A(z,t)\}$, and $\tilde{E}(z,\omega) = [(]\tilde{A}(z,\omega) + \tilde{A}^*(z,-\omega)]/2$. Furnished with these definitions, they derive the propagation equation

$$\frac{\partial \tilde{A}}{\partial z} = i\left|\frac{\omega \mathrm{n}(\omega)}{c}\right|\tilde{A} + i\left|\frac{\omega}{c\mathrm{n}(\omega)}\right| \sum_{\omega_1+\omega_2+\omega_3=\omega} \chi^{(3)}(\omega,\omega_1,\omega_2,\omega_3)\tilde{E}(\omega_1)\tilde{E}(\omega_2)\tilde{E}(\omega_3). \tag{34}$$

This equation is similar to the GNLSE (*cf.* Eq. (26)), but it includes both the forward and backward propagating waves. This is indeed possible by appealing to $\tilde{E}$ in the second term. The authors of Ref. [125] then prove that the preceding equation conserves the photon number. However, they need to appeal to one key assumption: the nonlinear coefficient in Eq. (12) is symmetric with respect to all permutations of frequencies. As noted in Ref. [125], this is suggested by Miller's rule [147,148] (*cf.* Eq. (32); modal dispersion is not taken into account):

$$\tilde{\chi}^{(3)}(\omega,\omega_1,\omega_2,\omega_3) \propto \tilde{\chi}^{(1)}(\omega)\tilde{\chi}^{(1)}(\omega_1)\tilde{\chi}^{(1)}(\omega_2)\tilde{\chi}^{(1)}(\omega_3). \tag{35}$$

We refer the interested reader for details to Ref. [125].

2.6. Photon-conserving NLSE

Despite the remarkable success of the (G)NLSE in modeling light fields in optical fibers, its limitations become evident when dealing with media whose nonlinear response varies considerably with frequency. Blow et al. [90] have shown in 1989 that whenever the frequency dependence departs from the particular case if $\tilde{\gamma}(\Omega) = \gamma_0(\Omega+\omega_0)/\omega_0$, the GNLSE does not conserve the photon number, even when there are no losses. This specific form of the nonlinear parameter becomes a necessary condition because all other effects (linear dispersion, Kerr effect, Raman effect) do not alter the photon number. As discussed in this section, even though alternatives to the NLSE and GNLSE have been explored, the more general case of an arbitrary $\tilde{\gamma}(\Omega)$, whose dependence on frequency may arise either from a frequency-dependent nonlinear index n_2 or from a frequency-dependent effective area, was not considered prior to the introduction of the photon-conserving NLSE (pcNLSE), at least not in the form of that lends itself to efficient numerical calculations. We show in this subsection that the path followed to obtain the pcNLSE also paves the way to including other effects such as the inclusion of Raman scattering.

In very general terms, the pcNLSE appears as a special case of the quantum description for the propagation of radiation inside a waveguide such as an optical fiber. Once the quantum evolution have been properly described by resorting to a quantum picture of the processes such as dispersion and four-wave mixing (FWM), we expect that observations would reproduce the classical description on averaging. Since photon number is conserved by default in a quantum description, its conservation will be naturally inherited when going to the classical limit. One only has to pay special attention to what precise form of the evolution operators must be used to reproduce a given frequency dependence of the nonlinearity in the classical limit.

We first show how to derive the usual nonlinear Schrödinger equation, Eq. (16), for a lossless waveguide in a quantum-mechanical setting. Following the work of Lai and Haus [149], we start with the following evolution equation:

$$-\mathrm{i}\hbar\frac{\partial}{\partial z}|\Psi_z\rangle = \hat{P}|\Psi_z\rangle, \tag{36}$$

where $|\Psi_z\rangle$ represents the quantum state at a distance z inside the fiber for a given initial state $|\Psi_0\rangle$ at $z = 0$ and $\hat{P}$ is the propagation operator. Let $|\Psi_{z,\Omega}\rangle$, or just $|\Psi_\Omega\rangle$ when clear from the context, represent the state at a given frequency Ω in such a way that $|\Psi_z\rangle = \bigotimes_\Omega \Psi_{z,\Omega}$. Note that evolution occurs along the fiber's length, and that is why the conserved quantity measured by $\hat{P}$ is linear momentum (rather than energy as for the Schrödinger equation).

Quantization of electromagnetic fields is performed by resorting to an analogue between optical modes and harmonic oscillators [150,151]. Let us assume that the envelope $A(z,t)$ of the electric field in a single-mode fiber can be written as a periodic function with period T as

$$A(z,t) = \frac{1}{2\pi}\sum_{m\in\mathbb{Z}} \tilde{K}_m(z)e^{i\omega_0 t - im\Delta\Omega t}\Delta\Omega, \tag{37}$$

with $\Delta\Omega = 2\pi/T$. In the limit of a continuum frequency space, this equation corresponds to the inverse frequency Fourier transform and $\tilde{K}_m$ corresponds to $\tilde{K}(z,\Omega)$. Furnished with this understanding and with some abuse of notation, we proceed as if we were always working with a continuum, where $\Delta\Omega$ becomes $d\Omega$. The quantization is accomplished by defining the operators

$$\hat{K}(z,\Omega) = \sqrt{\frac{2\pi\hbar\omega}{d\Omega}}\hat{a}(z,\Omega)e^{i\omega t}, \qquad \hat{K}^\dagger(z,\Omega) = \sqrt{\frac{2\pi\hbar\omega}{d\Omega}}\hat{a}^\dagger(z,\Omega)e^{i\omega t}, \tag{38}$$

where $\hat{a}(z,\Omega)$ and $\hat{a}^\dagger(z,\Omega)$ are the usual lowering and raising ladder operators, which in turn can be related to the classical complex envelope $\tilde{K}(z,\Omega)$, and its complex conjugate $\tilde{K}^*(z,\Omega)$. This relation exhibits itself naturally when considering the classical energy density for each frequency Ω at a given z, $|\tilde{K}(z,\Omega)|^2$. Indeed,

$$\begin{aligned} |\tilde{K}(z,\Omega)|^2 &= \tilde{K}^*(z,\Omega)\tilde{K}(z,\Omega) = \left\langle \hat{K}^\dagger(z,\Omega)\hat{K}(z,\Omega)\right\rangle \\ &= \frac{2\pi\hbar\omega}{d\Omega}\langle\Psi|\hat{a}^\dagger(z,\Omega)\hat{a}(z,\Omega)|\Psi\rangle \\ &= \frac{2\pi\hbar\omega n_\Omega}{d\Omega}, \end{aligned} \tag{39}$$

where we have used the fact that $a^\dagger a|\Psi\rangle = \hat{n}_\Omega|\Psi\rangle$, with n_Ω the photon number.

The NLSE can then be written in the frequency domain as the evolution of the mean

$$\begin{aligned} \frac{\partial}{\partial z}\left\langle \hat{K}(z,\Omega)\right\rangle &= \mathrm{i}\tilde{\beta}(\Omega)\left\langle \hat{K}_\Omega\right\rangle + \mathrm{i}\tilde{\gamma}(\Omega)\left\langle \mathcal{F}\{|K(z,t)|^2K(z,t)\}\right\rangle \\ &= \mathrm{i}\tilde{\beta}(\Omega)\left\langle \hat{K}_\Omega\right\rangle + \mathrm{i}\iint_{\mathbb{R}^2} d\omega_1 d\omega_2 \frac{\tilde{\gamma}(\Omega)}{(2\pi)^2}\left\langle \hat{K}^\dagger_{\omega_1}\hat{K}_{\Omega-\omega_2}\hat{K}_{\omega_1+\omega_2}\right\rangle. \end{aligned} \tag{40}$$

Given that $\partial_z\left\langle \hat{K}_\Omega\right\rangle = \frac{\mathrm{i}}{\hbar}\left\langle[\hat{K}_\Omega,\hat{P}]\right\rangle$, it follows that

$$[\hat{K}_\Omega,\hat{P}] = \hbar\tilde{\beta}(\Omega)\hat{K}_\Omega + \frac{\hbar\tilde{\gamma}(\Omega)}{(2\pi)^2}\iint_{\mathbb{R}^2} d\omega_1 d\omega_2\left\langle \hat{K}^\dagger_{\omega_1}\hat{K}_{\Omega-\omega_2}\hat{K}_{\omega_1+\omega_2}\right\rangle, \tag{41}$$

together with the hermiticity $\hat{P} = \hat{P}^\dagger$. The right side of Eq. (41) suggests that $\hat{P}$ should be decomposed as $\hat{P} = \hat{P}_{\mathrm{D}} + \hat{P}_{\mathrm{FWM}}$, where the linear contribution is due to chromatic dispersion and the nonlinear contribution is due to four-wave mixing (FWM). Since the momentum of a photon of energy $\hbar(\Omega+\omega_0)$ is given by $\hbar\tilde{\beta}(\Omega)$, if there are n_Ω photons per mode, it is natural to propose

$$\hat{P}_{\mathrm{D}} = \int_{\mathbb{R}} d\Omega'\hbar\tilde{\beta}(\Omega')\hat{n}_{\Omega'} = \int_{\mathbb{R}} d\Omega'\frac{\tilde{\beta}(\Omega')}{2\pi(\Omega'+\omega_0)}\hat{K}^\dagger_{\Omega'}\hat{K}_{\Omega'}. \tag{42}$$

Hermiticity of $\hat{P}_{\mathrm{D}}$ results from the fact that $\tilde{\beta}(\Omega)$ is real valued in a lossless waveguide. Also, as expected,

$$\begin{aligned} [\hat{K}_\Omega,\hat{P}_{\mathrm{D}}] &= \int_{\mathbb{R}}\frac{\tilde{\beta}(\Omega')[\hat{K}_\Omega,\hat{K}^\dagger_{\Omega'}]\hat{K}_{\Omega'}}{2\pi(\Omega'+\omega_0)}d\Omega' \\ &= \int_{\mathbb{R}}\hbar\tilde{\beta}(\Omega')\delta(\Omega-\Omega')\hat{K}_{\Omega'}d\Omega' = \hbar\tilde{\beta}(\Omega)\hat{K}_\Omega, \end{aligned} \tag{43}$$

It is not easy to deduce the form of $\hat{P}_{\mathrm{FWM}}$ since new frequencies are produced during a FWM process. Nevertheless, FWM can be thought as a process where two photons of frequencies ω_1 and ω_2 are annihilated while two new photons are created at frequencies ω_3 and ω_4 such that $\omega_1+\omega_2 = \omega_3+\omega_4$. In terms of ladder operators, FWM then can be pictured as $\hat{a}^\dagger_{\Omega_1}\hat{a}^\dagger_{\Omega_2}\hat{a}_{\Omega_1-\Omega'}\hat{a}_{\Omega_2-\Omega'}$. We thus propose the form

$$\hat{P}_{\mathrm{FWM}} = \kappa\iiint_{\mathbb{R}^3} d\Omega_1 d\Omega_2 d\Omega'\hat{K}^\dagger_{\Omega_1}\hat{K}^\dagger_{\Omega_2}\hat{K}_{\Omega_1-\Omega'}\hat{K}_{\Omega_2+\Omega'}, \tag{44}$$

where κ is to be determined. With a simple change of variables it is easy to show that $\hat{P}_{\mathrm{FWM}} = \hat{P}^\dagger_{\mathrm{FWM}}$ whenever κ is a real number. Straightforward calculations yield

$$[\hat{K}_\Omega,\hat{P}_{\mathrm{FWM}}] = 4\pi\hbar\omega\kappa\iint_{\mathbb{R}^2} d\Omega_1 d\Omega'\hat{K}^\dagger_{\Omega_1}\hat{K}^\dagger_{\Omega_1+\Omega'}\hat{K}_{\Omega-\Omega'}. \tag{45}$$

To recover the expression given by the NLSE in Eq. (16), it suffices to choose $\kappa = \gamma_0/(16\pi^3\omega_0)$. Thus, the following form for the propagation operator,

$$\hat{P} = \int_{\mathbb{R}} d\Omega'\frac{\tilde{\beta}(\Omega')}{2\pi(\Omega'+\omega_0)}\hat{K}^\dagger_{\Omega'}\hat{K}_{\Omega'}$$

$$+\frac{\gamma_0}{16\pi^3\omega_0}\iiint_{\mathbb{R}^3} d\Omega_1 d\Omega_2 d\Omega' \hat{K}^\dagger_{\Omega_1}\hat{K}^\dagger_{\Omega_2}\hat{K}_{\Omega_1-\Omega'}\hat{K}_{\Omega_2-\Omega'}, \tag{46}$$

provides a quantum description of light propagation inside fiber, when dispersion and FWM are considered. Its use leads to the NLSE in the classical limit with $\tilde{\gamma}(\Omega) \simeq \gamma_0$.

An important question is how $\hat{P}$ should look like when the effect of self-steepening is not negligible, and $\tilde{\gamma}(\Omega)$ cannot be considered a constant. One might consider making κ in Eq. (44) a function of frequency (we have already discussed a similar approach in Section 2.4). There are, in fact, four frequencies involved and κ should depend on all of them. This arguments leads to

$$\hat{P}_{\mathrm{FWM}} = \iiint_{\mathbb{R}^3} d\Omega_1 d\Omega_2 d\Omega_3\ \kappa(\Omega_1,\Omega_2,\Omega_1-\Omega_3,\Omega_2+\Omega_3) \\ \times \hat{K}^\dagger_{\Omega_1}\hat{K}^\dagger_{\Omega_2}\hat{K}_{\Omega_1-\Omega_3}\hat{K}_{\Omega_2+\Omega_3}. \tag{47}$$

The hermiticity now imposes the condition

$$\kappa(\Omega_1,\Omega_2,\Omega_3,\Omega_4) = \kappa^*(\Omega_4,\Omega_3,\Omega_2,\Omega_1). \tag{48}$$

Following Ref. [125], we use a more stringent condition that also guarantees hermiticity:

$$\kappa(\Omega_1,\Omega_2,\Omega_3,\Omega_4) = \mathrm{Re}\left\{\phi(\Omega_1)\phi(\Omega_2)\phi(\Omega_3)\phi(\Omega_4)\right\}, \tag{49}$$

where $\phi(\Omega)$ is a possibly complex function of the frequency. Eq. (49) can be considered a generalization of Miller's rule [147,148]. The FWM operator now becomes

$$\hat{P}_{\mathrm{FWM}} = \frac{1}{2}\iiint_{\mathbb{R}^3} d\Omega_1 d\Omega_2 d\Omega_3 \hat{V}^\dagger_{\Omega_1}\hat{V}^\dagger_{\Omega_2}\hat{U}_{\Omega_1-\Omega_3}\hat{U}_{\Omega_2+\Omega_3} + \\ \frac{1}{2}\iiint_{\mathbb{R}^3} d\Omega_1 d\Omega_2 d\Omega_3 \hat{U}^\dagger_{\Omega_1}\hat{U}^\dagger_{\Omega_2}\hat{V}_{\Omega_1-\Omega_3}\hat{V}_{\Omega_2+\Omega_3}, \tag{50}$$

with $\hat{U}_\Omega = \phi(\Omega)\hat{K}_\Omega$ and $\hat{V}_\Omega = \phi^*(\Omega)\hat{K}_\Omega$.

We need to choose the function $\phi(\Omega)$ such that it reproduces correctly the frequency dependence of $\tilde{\gamma}(\Omega)$. For this purpose, it suffices to restrict to a scenario where the NLSE and the new equation coincide: that of a monochromatic wave that only suffers from self-phase modulation (SPM). This approach yields $\phi(\Omega) = \sqrt[4]{\tilde{\gamma}(\Omega)/(2(2\pi)^3\hbar\omega)}$. Using this form, we arrive at the so-called photon-conserving NLSE

$$\frac{\partial \tilde{K}(z,\Omega)}{\partial z} = \mathrm{i}\tilde{\beta}(\Omega)\tilde{K}(z,\Omega) + \frac{\mathrm{i}}{2}(\omega_0+\Omega)\,\tilde{\Gamma}(\Omega)\mathcal{F}\{V^*(z,T)U^2(z,T)\} \\ + \frac{\mathrm{i}}{2}(\omega_0+\Omega)\,\tilde{\Gamma}^*(\Omega)\mathcal{F}\{U^*(z,T)V^2(z,T)\}, \tag{51}$$

where

$$\tilde{\Gamma}(\Omega) = \sqrt[4]{2(2\pi)^3\hbar}\phi(\Omega) = \sqrt[4]{\frac{\tilde{\gamma}(\Omega)}{\omega_0+\Omega}}, \tag{52}$$

$U(z,T) = \mathcal{F}^{-1}\{\tilde{U}(z,\Omega)\}$, and $V(z,T) = \mathcal{F}^{-1}\{\tilde{V}(z,\Omega)\}$ with

$$\tilde{U}(z,\Omega) = \tilde{\Gamma}(\Omega)\tilde{K}(z,\Omega), \qquad \tilde{V}(z,\Omega) = \tilde{\Gamma}^*(\Omega)\tilde{K}(z,\Omega). \tag{53}$$

To stress the importance of our new photon-conserving NLSE, we perform numerical simulations for three scenarios. We launch a $T_0 = 0.1$ ps Gaussian pulse with a peak power $P_0 = 200$ W and a central frequency ω_0 corresponding to the wavelength of 1550 nm in a fiber with negligible chromatic dispersion and $\tilde{\gamma}(\Omega) = \gamma_0 + \gamma_1\Omega$. We choose $\gamma_0 = 1.2\times10^{-3}\ \mathrm{W}^{-1}\mathrm{m}^{-1}$ but use three different values: $\gamma_1 = \gamma_0/\omega_0$, $\gamma_1 = 2\gamma_0/\omega_0$, and $\gamma_1 = -\gamma_0/\omega_0$. The numerical results are shown in Fig. 3. Left panels show the input and output pulses for the NLSE and the pcNLSE, while right panels show the photon number as a function of distance in terms of the shock length $z_{\mathrm{shock}} = 0.39\ T_0/(|\gamma_1|P_0)$. For $\gamma_1 = \gamma_0/\omega_0$ (top panels), results coincide as expected. Nevertheless, for $\gamma_1 = 2\gamma_0/\omega_0$ and $\gamma_1 = -\gamma_0/\omega_0$ (middle and bottom panels), results differ significantly, and the necessary condition of photon conservation is only obeyed by the pcNLSE.

2.6.1. *Photon-conserving GNLSE*

Eq. (51) does not include the effect of linear losses or that of Raman scattering. For including such lossy processes, we need to consider an open quantum system, leading to the so-called Lindblad formulation [99,150,151]

$$\hbar\frac{d\rho}{dz} = \mathrm{i}\left[\hat{P},\rho\right] + \sum_{m\in\mathbb{Z}} \hat{L}^{(\mathrm{l})}\rho\hat{L}^{\dagger(\mathrm{l})} - \frac{1}{2}\left\{\rho, \hat{L}^{\dagger(\mathrm{l})}\hat{L}^{(\mathrm{l})}\right\} \\ + \sum_{m\in\mathbb{Z}} \hat{L}^{(\mathrm{R})}\rho\hat{L}^{\dagger(\mathrm{R})} - \frac{1}{2}\left\{\rho, \hat{L}^{\dagger(\mathrm{R})}\hat{L}^{(\mathrm{R})}\right\}, \tag{54}$$

where ρ is the density matrix of the mixed quantum state, and $\hat{L}^{(\mathrm{l})}$ and $\hat{L}^{(\mathrm{R})}$ are the Lindblad operators [152] for linear loss and Raman scattering, respectively. Observe that the inclusion of other lossy phenomena, such as two-photon absorption [153], can be

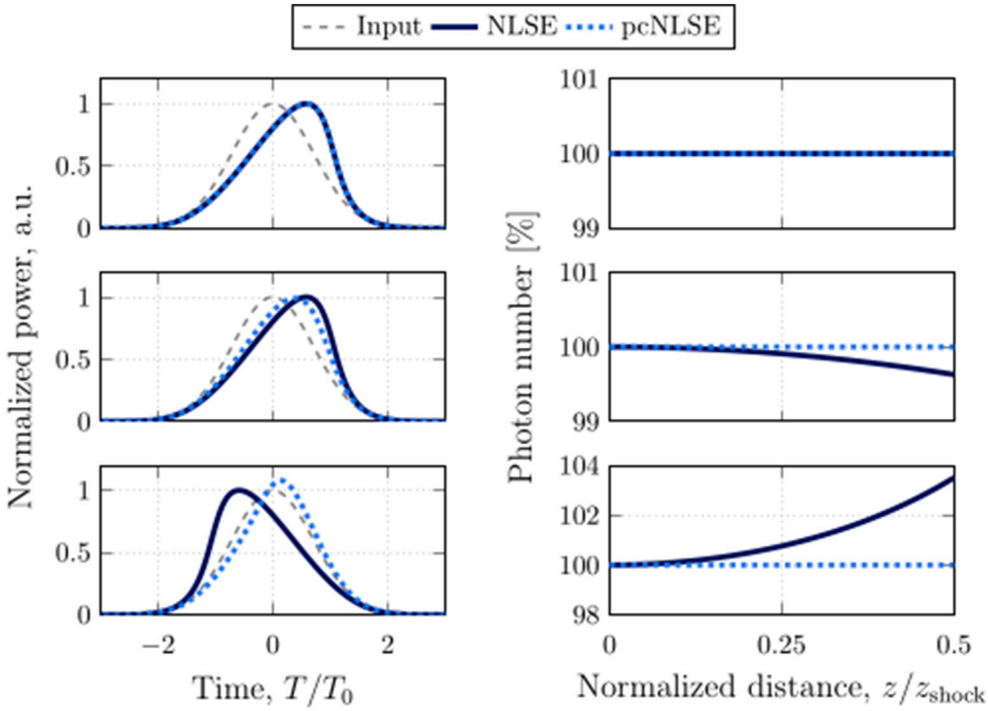

Fig. 3. A $T_0 = 0.1$ ps Gaussian pulse with a peak power $P_0 = 200$ W and a central frequency ω_0, corresponding to the wavelength of 1550 nm, is launched in a fiber with negligible chromatic dispersion and $\tilde{\gamma}(\Omega) = \gamma_0 + \gamma_1 \Omega$, $\gamma_0 = 1.2 \times 10^{-3}$. Pulse shapes (left) and photon-number evolution (right) obtained using the NLSE and the pcNLSE for three values of the self-steepening parameter: $\gamma_1 = \gamma_0/\omega_0$ (top row), $\gamma_1 = 2\gamma_0/\omega_0$ (middle row) and $\gamma_1 = -\gamma_0/\omega_0$ (bottom row). The shock length is given by $z_{\mathrm{shock}} = 0.39\ T_0/(|\gamma_1|P_0)$.

done in a similar fashion. The momentum operator in Eq. (46) has to be modified to incorporate the conserving (hermitian) part of the Raman interaction as $\hat{P} = \hat{P}_{\mathrm{D}} + \hat{P}_{\mathrm{FWM}} + \hat{P}_{\mathrm{R}}$, where

$$\hat{P}_{\mathrm{R}} = \iiint_{\mathbb{R}^3} d\Omega_1 d\Omega_2 d\Omega' \, \frac{\gamma_0 f^{(\mathrm{R})} \mathrm{Re}\left\{ \tilde{h}^{(\mathrm{R})}_{\Omega'} \right\}}{4\pi\omega_0} \hat{K}^{\dagger}_{\Omega_1} \hat{K}^{\dagger}_{\Omega_2} \hat{K}_{\Omega_1-\Omega'} \hat{K}_{\Omega_2+\Omega'}, \tag{55}$$

in the limit of a continuous spectrum, $f^{(\mathrm{R})}$ is the fractional Raman contribution, and $\tilde{h}^{(\mathrm{R})}$ is the normalized Raman response [6]. The Lindblad operators can be shown to be [99,150,151]

$$\hat{L}^{(\mathrm{l})} = \sqrt{\frac{\tilde{\alpha}_{\Omega}}{\omega_0 + \Omega}} \hat{K}, \tag{56}$$

$$\hat{L}^{(\mathrm{R})} = \int_{\mathbb{R}} d\Omega' \sqrt{\frac{\gamma_0 f^{(\mathrm{R})} \mathrm{Im}\left\{ \tilde{h}^{(\mathrm{R})}_{\Omega} \right\}}{\pi\omega_0}} \hat{K}^{\dagger}_{\Omega'-\Omega} \hat{K}_{\Omega'}, \tag{57}$$

where $\tilde{\alpha}$ is the frequency-dependent linear loss. Some simple but lengthy calculations lead to the so-called photon-conserving GNLSE (pcGNLSE):

$$\begin{aligned}
\frac{\partial \tilde{K}(z,\Omega)}{\partial z} &= + \mathrm{i}\tilde{\beta}(\Omega)\tilde{K}(z,\Omega) - \frac{\tilde{\alpha}(\Omega)}{2}\tilde{K}(z,\Omega) \\
&+ \mathrm{i}\frac{(\omega_0+\Omega)\,\tilde{\Gamma}(\Omega)}{2}\mathcal{F}\{V^*(z,T)U^2(z,T)\} \\
&+ \mathrm{i}\frac{(\omega_0+\Omega)\,\tilde{\Gamma}^*(\Omega)}{2}\mathcal{F}\{U^*(z,T)V^2(z,T)\} \\
&+ \mathrm{i}f^{(\mathrm{R})}(\omega_0+\Omega)\,\tilde{\Gamma}^*(\Omega)\mathcal{F}\{U(z,t)\int_0^{\infty} d\tau h^{(\mathrm{R})}(\tau)|U(z,t-\tau)|^2\} \\
&- \mathrm{i}f^{(\mathrm{R})}(\omega_0+\Omega)\,\tilde{\Gamma}^*(\Omega)\mathcal{F}\{U(z,t)|U(z,t)|^2\}.
\end{aligned} \tag{58}$$

With the use of GNLSE not only photon conservation would fail but also predictions would be different both quantitatively and qualitatively. For instance, for media with negative nonlinear coefficients, the GNLSE predicts an unphysical Raman-induced blue shift, while the pcGNLSE predicts the usual red shift. Furthermore, the pcGNLSE can be efficiently solved with the same numerical algorithms as the GNLSE [154,155].

2.6.2. Some consequences of the pcNLSE

Linale et al. [103,156] studied differences in the predictions made by the NLSE and the pcNLSE for the phenomenon of modulation instability (MI). One interesting result is related to the cutoff power (COP) of the MI found in the presence of self-steepening. It has been shown that the MI gain ceases to exist when input pump power exceeds a critical value [157–159]. The analysis based on the pcNLSE, however, reveals that are parameter regions where this cutoff is suppressed, leading to MI with either a narrowband or ultrawide gain spectrum, depending on the sign of γ_1.

It is interesting to note that even soliton solutions of the NLSE do not conserve the number of photons [160]. Hernandez et al. [102] analyzed the existence of solitons under the pcNLSE. It turns out that one can obtain approximate analytic expressions for solitons when the sign of $\tilde{\gamma}(\Omega)$ does not change. Indeed, it is simple to show that for $\tilde{\gamma}(\Omega) > 0$ the pcNLSE can be written as

$$\frac{\partial \tilde{U}(z,\Omega)}{\partial z} = \mathrm{i}\tilde{\beta}'(\Omega)\tilde{B}(z,\Omega) + \mathrm{i}\sqrt{(\omega_0+\Omega)\tilde{\gamma}(\Omega)}\mathcal{F}\{U(z,t)|U(z,t)|^2\}, \tag{59}$$

A similar expression can be obtained for $\tilde{\gamma}(\Omega) < 0$. Further insight into the photon-conserving NLSE can be obtained by noting, as explained in Ref. [102], that one can use the following approximation in the narrowband case:

$$\begin{aligned}\frac{\partial \tilde{K}(z,\Omega)}{\partial z} \approx{}& i\tilde{\beta}'(\Omega)\tilde{K}(z,\Omega) + i\gamma_0\left(1+\frac{\Omega}{\omega_0}\right)\mathcal{F}\{K(z,t)|K(z,t)|^2\}\\ &-\left(\gamma_1-\frac{\gamma_0}{\omega_0}\right)\mathcal{F}\{|K(z,t)|^2\frac{\partial K(z,t)}{\partial t}\}.\end{aligned} \tag{60}$$

This approximation reduces to the usual NLSE when $\gamma_1 = \gamma_0/\omega_0$, which is the only case in which the NLSE conserves the photon number.

Linale et al. [100] extended the study of soliton-like pulses to the pcGNLSE. In particular, using the method of moments [161–163] for positive $\tilde{\gamma}(\Omega)$, it was found that an initial sech-shape pulse evolves as

$$K(z,t) = k_p \mathrm{sech}\left(\frac{T-q_p}{T_p}\right)\exp\left\{-\Omega_p(T-q_p) - iC_p\frac{(T-q_p)^2}{2T_p^2} + i\phi_p\right\}, \tag{61}$$

where Ω_p is the soliton's frequency shift and q_p is the temporal delay induced by this spectral shift. These parameters are found to be (see Appendix A in Ref. [100]):

$$\Omega_p = -\frac{8T_\mathrm{R}\gamma_0 P_0}{15T_0^2}z, \qquad q_p = \frac{\beta_2\Omega_p}{2}z + \frac{\left(\gamma_1\frac{\omega_0}{\gamma_0}+2\right)\gamma_0 P_0}{3\omega_0}z, \tag{62}$$

where T_R is the effective Raman parameter (see Chapter 2 of Agrawal [6]) and P_0 is the initial peak power. It is interesting to compare these expressions with the analog ones for solitons under the NLSE [162,163]. The frequency shift Ω_p does not change. However, the delay is significantly different. In the case of the pcGNLSE, the effect of the self-steepening disappears when $\gamma_1 = -2\gamma_0/\omega_0$. Furthermore, measurements of q_p enable the estimation of the value of γ_0. For more details, the reader is referred to Ref. [100]. Refs. [101,164] present alternative methods for measuring the self-steepening parameter.

The results in this section assume that the sign of the nonlinear coefficient $\tilde{\gamma}(\Omega)$ does not change over the entire frequency range. A more interesting scenario corresponds to the case where the sign of $\tilde{\gamma}(\Omega)$ changes at a specific wavelength known as the zero-nonlinearity wavelength (ZNW). This case is analyzed in the next section.

3. Impact of a ZNW and a ZDW

In this section, we present some recent results on the influence of the zero-dispersion and the zero-nonlinearity wavelengths on the propagation of pulses. In particular, Section 3.1 delves in the influence of the zero-nonlinearity wavelength on the propagation of solitons. Section 3.2 studies the collision of a strong pulse with a much weaker pulse in the presence of a ZNW. Using the temporal analogy of the reflection and refraction phenomena, it is explained how a weaker pulse can be used to control a stronger, pump, pulse, with applications, *e.g.*, in all-optical switching.

3.1. Influence of a ZNW on solitons

In the work of Bose et al. [83], the influence of both the ZNW and the ZDW on the propagation of solitons in a silver-doped PCF was studied. They found that the Raman-induced red shift of a fundamental soliton is reduced when the ZNW is longer compared to that of the soliton, effectively acting as a barrier. Moreover, the relative positions of the ZNW and the ZDW give rise to separate solitonic and non-solitonic spectral regions with significantly different pulse dynamics, even producing different kinds of dispersive waves. In another study, Bose et al. [82] showed how the interplay between dispersion and a large negative nonlinearity, achieved in a PCF doped with silver nanoparticles, results in a blue shift of solitons. They also analyzed the role of self-steepening in the generation of dispersive waves. Building upon this work, Arteaga-Sierra et al. [79] showed the enhancement and suppression of the Raman-induced frequency shift of fundamental solitons and dispersive waves, depending on the magnitude of the self-steepening

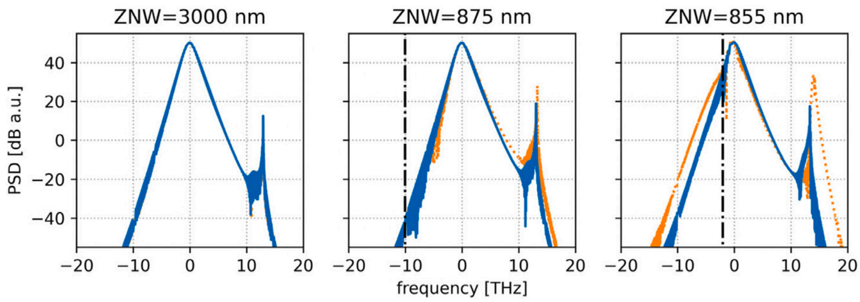

Fig. 4. Dependence of output spectra on the ZNW (adapted from Ref. [166]) when the NLSE (dotted orange curve) or GNLSE (solid blue curve) is employed for soliton's propagation. The ZNW is indicated by a black line. (For interpretation of the references to color in this figure legend, the reader is referred to the web version of this article.)

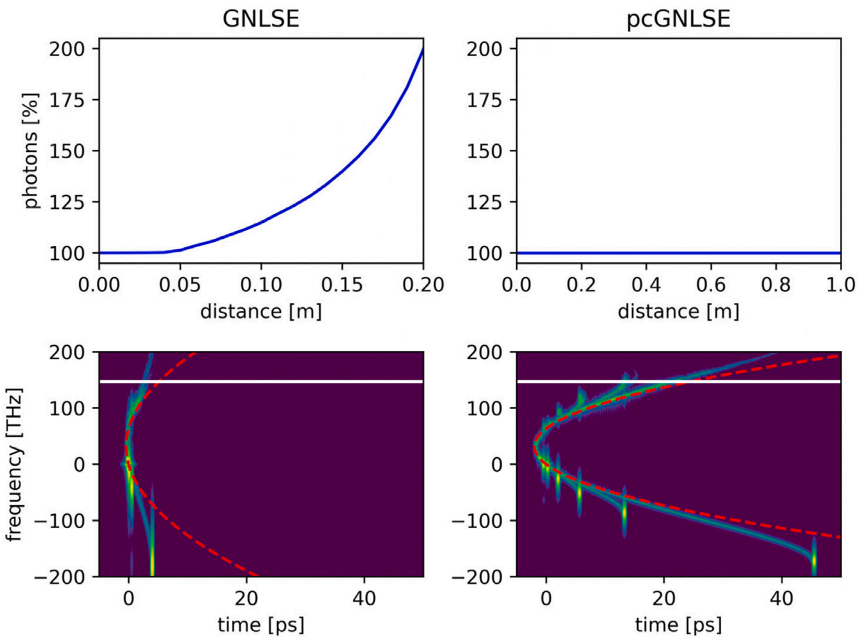

Fig. 5. Changes with distance in the number of photons (top) and corresponding spectrograms (bottom) obtained using the GNLSE (left) and the pcGNLSE (right) [166]. The ZNW lies at 600 nm for these numerical simulations.

parameter $s = \gamma_1/(\gamma_0/\omega_0)$. They also showed the propagation of solitons in the normal dispersion regime, made possible by the existence of a ZNW, and explored pulse dynamics for different relative positions of the ZNW and the ZDW.

Zhao et al. [81] studied the evolution of higher-order solitons propagating in an all-normal dispersion (ANDi) PCF doped with silver nanoparticles and exhibiting a strong frequency-dependent nonlinearity. They argue that the existence of a ZNW and tunability of the frequency dependence of the nonlinear parameter provide a degree of freedom in regulating the spectral shift and energy distribution of the fundamental soliton and dispersive waves. Similarly, in Ref. [165], Zhao et al. extended the study of the effect of the ZNW and the ZDW on the propagation of higher-order solitons. As in previous cases, they reported a blue shift of the fundamental soliton satisfying phase-matching and group-velocity-matching conditions. Further, they reported on the tunneling experienced by the soliton through a spectrally limited non-solitonic region.

In a recent study, Hernandez et al. [166] analyzed the behavior of Cherenkov radiation when the soliton is launched at the wavelength $\lambda_0 = 850$ nm, but the ZNW varies over a wide range; their results are shown in Fig. 4. When the ZNW lies far from λ_0 ($\lambda_{\text{ZNW}} = 3000$ nm), both the NLSE and the pcNLSE yield similar results, in agreement with the theoretical prediction. However, the use of the photon-conserving equation is required when the ZNW is close to the soliton, as seen clearly in the central and the right panel of Fig. 4 for $\lambda_{\text{ZNW}} = 875$ nm and $\lambda_{\text{ZNW}} = 855$ nm, respectively. In those cases, both the amplitude and frequency of Cherenkov radiation exhibit different results for the NLSE and pcNLSE. The use of the pcNLSE is essential for accurately predicting the frequency of the Cherenkov radiation ($\lambda_{\text{Ch}} \approx 820$ nm).

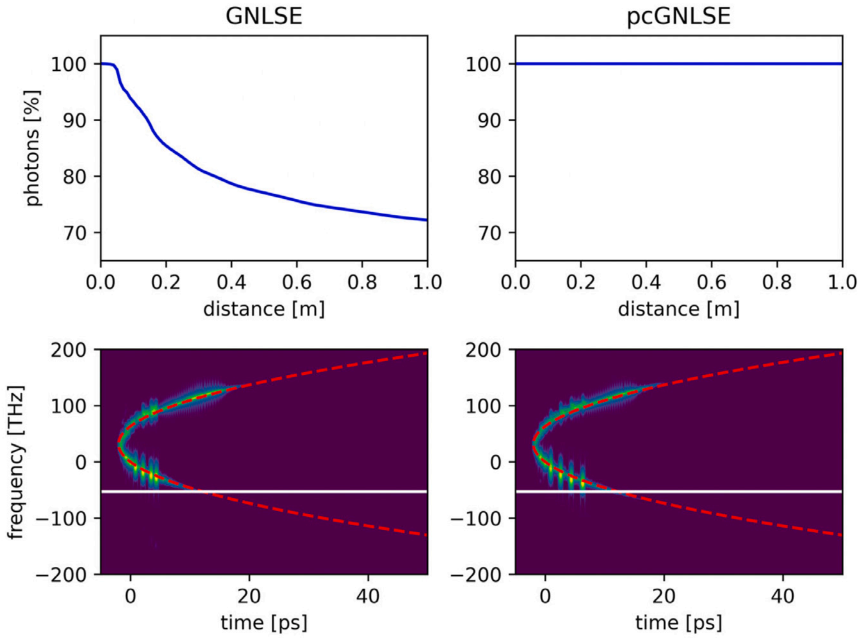

Fig. 6. Changes with distance in the number of photons (top) and corresponding spectrograms (bottom) obtained using the GNLSE (left) and the pcGNLSE (right) [166]. The ZNW lies at 1000 nm for these numerical simulations.

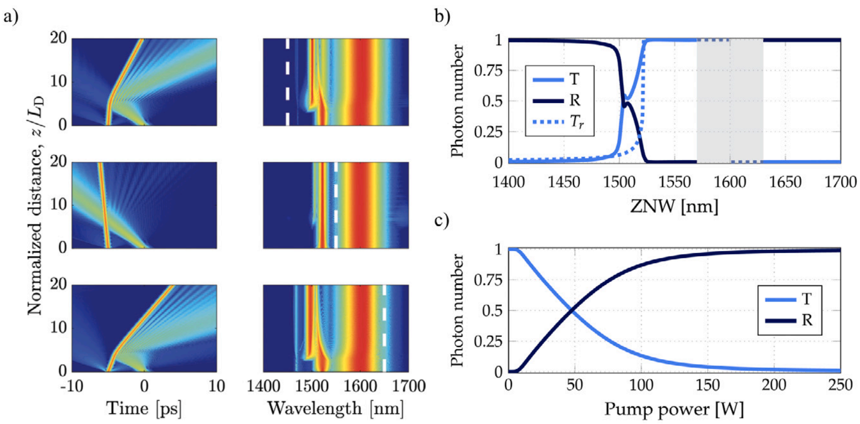

Fig. 7. Interaction between a soliton (pump) and a weak signal for three values of the ZNW [167]. (a) The signal is mostly reflected with a large frequency shift when the ZNW is 1450 nm (top) or 1650 nm (bottom), but is fully transmitted when the ZNW is at 1550 nm (center). (b) An analysis of the photon number identifies three regions of transmission, T, or reflection, R. T_r is the result of the analytical model in Ref. [167]. (c) Dependence of T and R on pump power.

Hernandez et al. also studied the dynamics of trapped radiation, arising from the propagation of a 9th-order soliton, by using the pcGNLSE to guarantee strict conservation of the number of photons. They showed that the influence of the ZNW becomes significant as the soliton's spectrum red shifts and the trapped radiation's blue shift is strongly affected depending on whether the ZNW lies on the blue or the red side of the soliton. Fig. 5 shows the trapped radiation when the ZNW is on the red side of the soliton, *i.e.*, when $\lambda_{\text{ZNW}} = 600$ nm, and Fig. 6 shows this when it lies at the blue side of the soliton, *i.e.*, when $\lambda_{\text{ZNW}} = 1000$ nm. Although the dynamics might appear similar when looking at the spectrograms, top panels display the evolution of the photon number. The NLSE is found to produce unphysical results in terms of the conservation of the number of photons. Further analysis for the relative positions of the ZDW and the ZNW was carried out by Melchert et al. in Ref. [89]. The authors looked at non-coherent coupled pulses in a medium with a ZNW and found the formation of photonic meta-atoms and molecule-like bound-states of pulses.

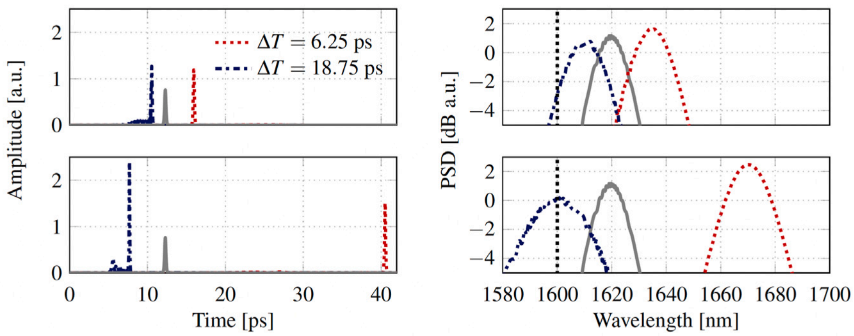

Fig. 8. Temporal and wavelength shifts of the soliton when the ZNW lies at 1450 nm and the peak power of the control pulse is 10 W (top) or 20 W (bottom). The Raman-induced frequency shift is suppressed or enhanced depending on control-pulse parameters. Input soliton and its spectrum are shown in gray.

3.2. Collision of pulses in the presence of a ZWN

The influence of the ZNW of a nonlinear medium on the interaction between an intense soliton and a weak signal pulse was studied by Sparapani et al. [167] using a model that relies on the temporal analogy of reflection and refraction put forth in Ref. [168]. Within a photon-number conserving frame, the signal's evolution is governed by

$$\frac{\partial}{\partial_z}\mathcal{K}_{\rm sig} + \bar{\beta}_1 \frac{\partial}{\partial t}\mathcal{K}_{\rm sig} + \mathrm{i}\frac{\bar{\beta}_2}{2}\frac{\partial^2}{\partial t^2}\mathcal{K}_{\rm sig} = \mathrm{i}\overline{\gamma}P(t)\mathcal{K}_{\rm sig}, \tag{63}$$

where $\mathcal{K}_{\rm sig}(z,t) = K_{\rm sig}(z,t)e^{-\mathrm{i}\bar{\beta}(\Omega_{\rm sig})z+\mathrm{i}\Omega_{\rm sig}t}$, $\Omega_{\rm sig}$ is the frequency shift of the signal from the pump, $\bar{\beta}_1 = \beta'(\Omega_{\rm sig})$, $\bar{\beta}_2 = \beta''(\Omega_{\rm sig})$, $P(t) = |K_{\rm pump}(t)|^2$, and the nonlinear coefficient is given by

$$\overline{\gamma} = 2\,\mathrm{Re}\left\{\sqrt{\gamma_0\,\tilde{\gamma}(\Omega_{\rm sig})(\omega_0+\Omega_{\rm sig})/\omega_0}\right\}. \tag{64}$$

As seen in Eq. (64), when γ_0 and $\tilde{\gamma}(\Omega_{\rm sig})$ have the same signs, the nonlinear coefficient $\overline{\gamma}$ has a finite value. In contrast, when they have opposite signs, $\overline{\gamma}$ vanishes. In the former case, the weak pulse undergoes a reflection when it collides with the soliton. In the latter case, the two pulses do not interact nonlinearly, and the weak pulse should be transmitted without any temporal reflection. Numerical results shown in Fig. 7 confirm this behavior when the relative position of the ZNW is varied in the range of 1450–1650 nm. As seen there, when the ZNW lies in between the wavelengths of two pulses, the signal is fully transmitted (center panel in part a). In contrast, when the ZNW lies on the blue side of the signal (top panel) or on the red side of the soliton (bottom panel), the signal is mostly reflected.

The transmitted and reflected regions described in Ref. [167] and seen in Fig. 7 depend on the spectral location of the ZNW, which can be treated as a design parameter, as shown in part (b) of Fig. 7. Given a fiber design with a certain ZNW, an all-optical switching scheme can be implemented by changing the soliton's peak power, as suggested in part (c) of Fig. 7.

Melchert et al. [169] have discussed how a control pulse launched with much less power than that of a pump can affect the evolution of the intense pump pulse. This behavior is analogous to that of a transistor. Based on this concept, Sparapani et al. [170] have recently analyzed how a weak control pulse, launched into an optical fiber at a different wavelength than that of the pump pulse, can affect the pump pulse both spectrally and temporally and how such changes can be controlled by adjusting the initial delay (ΔT) between the two pulses. They studied the influence of the ZNW over the extent of such nonlinear control and how the arrival time and frequency shifts of the pump pulses could be altered by changing parameters of the control pulse. Fig. 8 shows the results of numerical simulations for a pump pulse that propagates as a soliton inside an optical fiber and a control pulse is used to change its properties. The results are shown for two values of the initial delay, ΔT, between the two pulses. The soliton experiences a blue shift when $\Delta T = 18.75$ ps and a red-shift when $\Delta T = 6.25$ ps, and its arrival time at the fiber's output is also affected accordingly. The arrival time can be further tuned by changing peak power of the control pulse power. The peak power is 10 W in the top panels and is changed to 20 W in the bottom panels. Notice that the frequency shift induced by the control pulse can suppress or enhance the Raman-induced red shift of the soliton. An optical filter at the fiber's output can convert such spectral changes into an optical switch where pump pulses are transmitted or blocked depending on whether a control pulse is launched or not at the fiber's input end. Thus, the presence of a ZNW in a dispersive nonlinear medium opens up the possibility of realizing an all-optical switching scheme.

4. Conclusions

We have provided a thorough review of pulse propagation in optical waveguides, whose nonlinear response varies with frequency so much that even the sign of the Kerr parameter n_2 may reverse at a specific wavelength known as the zero-nonlinearity wavelength. We first focused on the mathematical treatment of the frequency-dependent Kerr nonlinearity for propagation of short pulses in optical fibers. We revisited the theoretical framework required to deal with this feature within physical constraints, such as the conservation of the photon number, and discussed several approaches used to cope with the problem. In particular, we presented the photon-conserving nonlinear Schrödinger equation and its generalized version and applied them to the study of the propagation of short pulses in waveguides exhibiting a frequency-dependent nonlinearity. Furthermore, we emphasized the role of the zero-nonlinearity wavelength and its interplay with the zero-dispersion wavelength by pointing out their influence on nonlinear propagation, specifically that of solitons and the ensuing generation of Cherenkov radiation. Then, by resorting to a space–time analogy, we discussed the interaction of a weak control pulse with an intense soliton, a promising scheme for all-optical switching.

In this review, we have dealt with either theoretical results or numerical simulations. To the best of our knowledge, waveguides with a zero-nonlinearity wavelength are yet to be fabricated. Thus, this research area needs a strong effort on the experimental side so that theoretical predictions reported here can be corroborated. PCFs doped with metallic nanoparticles, as mentioned in Sections 1 and 3, represent a plausible approach towards fabrication of the waveguides with a ZNW, but other approaches may be developed in due time. In this direction, optical fibers are not the only choice. Indeed, as mentioned in Section 1, integrated waveguides, especially those decorated with 2D materials such as graphene, provide an alternative where a ZNW can be found, putting forth the power and versatility of integrated photonics into the realm of technologically relevant applications such as all-optical switching.

CRediT authorship contribution statement

A.C. Sparapani: Writing – review & editing, Writing – original draft, Investigation. **S.M. Hernandez:** Writing – review & editing, Writing – original draft, Investigation. **P.I. Fierens:** Writing – review & editing, Writing – original draft, Investigation. **D.F. Grosz:** Writing – review & editing, Writing – original draft, Supervision, Investigation. **Govind P. Agrawal:** Writing – review & editing, Writing – original draft, Supervision, Investigation.

Declaration of competing interest

The authors declare that they have no known competing financial interests or personal relationships that could have appeared to influence the work reported in this paper.

Data availability

No data was used for the research described in the article.

Acknowledgments

We acknowledge fruitful discussions with J. Bonetti, A. Sánchez, and N. Linale. Part of this work was supported by CONICET, Argentina, under project PIP 2021 11220200100566CO. A. C. Sparapani gratefully acknowledges support from the Fulbright Commission and the Ministry of Education of Argentina for his stay at the University of Rochester where part of this work was carried out.

References

[1] T. Miya, Y. Terunuma, T. Hosaka, T. Miyashita, Ultimate low-loss single-mode fibre at 1.55 μm, Electron. Lett. 4 (15) (1979) 106–108.
[2] E. Desurvire, J.R. Simpson, P. Becker, High-gain erbium-doped traveling-wave fiber amplifier, Opt. Lett. 12 (11) (1987) 888–890.
[3] L. Reekie, I. Jauncey, Low-noise erbium-doped fibre amplifier operating at 1.54 μm, Electron. Lett. 19 (23) (1987) 1026–1028.
[4] W.J. Miniscalco, Erbium-doped glasses for fiber amplifiers at 1500 nm, J. Lightwave Technol. 9 (2) (1991) 234–250.
[5] C.R. Giles, E. Desurvire, Modeling erbium-doped fiber amplifiers, J. Lightwave Technol. 9 (2) (1991) 271–283.
[6] G.P. Agrawal, Nonlinear Fiber Optics, sixth ed., Academic Press, 2019.
[7] B. Culshaw, A. Kersey, Fiber-optic sensing: A historical perspective, J. Lightwave Technol. 26 (9) (2008) 1064–1078.
[8] X. Bao, L. Chen, Recent progress in distributed fiber optic sensors, Sensors 12 (7) (2012) 8601–8639.
[9] R. Di Sante, Fibre optic sensors for structural health monitoring of aircraft composite structures: Recent advances and applications, Sensors 15 (8) (2015) 18666–18713.
[10] A. Barrias, J.R. Casas, S. Villalba, A review of distributed optical fiber sensors for civil engineering applications, Sensors 16 (5) (2016) 748.
[11] L. Schenato, A review of distributed fibre optic sensors for geo-hydrological applications, Appl. Sci. 7 (9) (2017) 896.
[12] Z. Ding, C. Wang, K. Liu, J. Jiang, D. Yang, G. Pan, Z. Pu, T. Liu, Distributed optical fiber sensors based on optical frequency domain reflectometry: A review, Sensors 18 (4) (2018) 1072.
[13] S. Girard, A. Morana, A. Ladaci, T. Robin, L. Mescia, J.-J. Bonnefois, M. Boutillier, J. Mekki, A. Paveau, B. Cadier, et al., Recent advances in radiation-hardened fiber-based technologies for space applications, J. Opt. 20 (9) (2018) 093001.
[14] L. Ren, T. Jiang, Z.-g. Jia, D.-s. Li, C.-l. Yuan, H.-n. Li, Pipeline corrosion and leakage monitoring based on the distributed optical fiber sensing technology, Measurement 122 (2018) 57–65.
[15] P. Lu, N. Lalam, M. Badar, B. Liu, B.T. Chorpening, M.P. Buric, P.R. Ohodnicki, Distributed optical fiber sensing: Review and perspective, Appl. Phys. Rev. 6 (4) (2019).
[16] Z. Zhan, Distributed acoustic sensing turns fiber-optic cables into sensitive seismic antennas, Seismol. Res. Lett. 91 (1) (2020) 1–15.
[17] M.F. Bado, J.R. Casas, A review of recent distributed optical fiber sensors applications for civil engineering structural health monitoring, Sensors 21 (5) (2021) 1818.
[18] R. Min, Z. Liu, L. Pereira, C. Yang, Q. Sui, C. Marques, Optical fiber sensing for marine environment and marine structural health monitoring: A review, Opt. Laser Technol. 140 (2021) 107082.

[19] G. Fernández, A.C. Sparapani, N. Linale, J.C. Benitez, D.F. Grosz, A proposal for linear and nonlinear discrete and distributed sensing of mechanical strain with graphene-decorated optical fibers, Opt. Fiber Technol., Mater. Devices Syst. 73 (2022) 103046.
[20] J.A. Giordmaine, R.C. Miller, Tunable coherent parametric oscillation in $LiNbO_3$ at optical frequencies, Phys. Rev. Lett. 14 (24) (1965) 973.
[21] S.E. Harris, Tunable optical parametric oscillators, Proc. IEEE 57 (12) (1969) 2096–2113.
[22] R. Baumgartner, R. Byer, Optical parametric amplification, IEEE J. Quantum Electron. 15 (6) (1979) 432–444.
[23] S. Brosnan, R. Byer, Optical parametric oscillator threshold and linewidth studies, IEEE J. Quantum Electron. 15 (6) (1979) 415–431.
[24] D.C. Edelstein, E.S. Wachman, C.-L. Tang, Broadly tunable high repetition rate femtosecond optical parametric oscillator, Appl. Phys. Lett. 54 (18) (1989) 1728–1730.
[25] R.C. Eckardt, C. Nabors, W.J. Kozlovsky, R.L. Byer, Optical parametric oscillator frequency tuning and control, J. Opt. Soc. Am. B 8 (3) (1991) 646–667.
[26] L.E. Myers, R. Eckardt, M.M. Fejer, R.L. Byer, W.R. Bosenberg, Multigrating quasi-phase-matched optical parametric oscillator in periodically poled $LiNbO_3$, Opt. Lett. 21 (8) (1996) 591–593.
[27] W.R. Bosenberg, A. Drobshoff, J.I. Alexander, L.E. Myers, R.L. Byer, Continuous-wave singly resonant optical parametric oscillator based on periodically poled $LiNbO_3$, Opt. Lett. 21 (10) (1996) 713–715.
[28] W.R. Bosenberg, A. Drobshoff, J.I. Alexander, L.E. Myers, R.L. Byer, 93% Pump depletion, 3.5-W continuous-wave, singly resonant optical parametric oscillator, Opt. Lett. 21 (17) (1996) 1336–1338.
[29] K. Vodopyanov, F. Ganikhanov, J. Maffetone, I. Zwieback, W. Ruderman, $ZnGeP_2$ optical parametric oscillator with 3.8–12.4-μm tunability, Opt. Lett. 25 (11) (2000) 841–843.
[30] C. Canalias, V. Pasiskevicius, Mirrorless optical parametric oscillator, Nat. Photon. 1 (8) (2007) 459–462.
[31] A. Marandi, N.C. Leindecker, V. Pervak, R.L. Byer, K.L. Vodopyanov, Coherence properties of a broadband femtosecond mid-IR optical parametric oscillator operating at degeneracy, Opt. Express 20 (7) (2012) 7255–7262.
[32] G. Marty, S. Combrié, F. Raineri, A. De Rossi, Photonic crystal optical parametric oscillator, Nat. Photon. 15 (1) (2021) 53–58.
[33] J. Lu, A. Al Sayem, Z. Gong, J.B. Surya, C.-L. Zou, H.X. Tang, Ultralow-threshold thin-film lithium niobate optical parametric oscillator, Optica 8 (4) (2021) 539–544.
[34] D. Mawet, G. Ruane, W. Xuan, D. Echeverri, N. Klimovich, M. Randolph, J. Fucik, J.K. Wallace, J. Wang, G. Vasisht, et al., Observing exoplanets with high-dispersion coronagraphy. II. Demonstration of an active single-mode fiber injection unit, Astrophys. J. 838 (2) (2017) 92.
[35] A. Shabat, V. Zakharov, Exact theory of two-dimensional self-focusing and one-dimensional self-modulation of waves in nonlinear media, Sov. Phys.—JETP 34 (1) (1972) 62.
[36] A. Hasegawa, F. Tappert, Transmission of stationary nonlinear optical pulses in dispersive dielectric fibers. I. Anomalous dispersion, Appl. Phys. Lett. 23 (3) (1973) 142–144.
[37] L.F. Mollenauer, R.H. Stolen, J.P. Gordon, Experimental observation of picosecond pulse narrowing and solitons in optical fibers, Phys. Rev. Lett. 45 (13) (1980) 1095.
[38] J. Knight, T. Birks, P.S.J. Russell, D. Atkin, All-silica single-mode optical fiber with photonic crystal cladding, Opt. Lett. 21 (19) (1996) 1547–1549.
[39] T.A. Birks, J.C. Knight, P.S.J. Russell, Endlessly single-mode photonic crystal fiber, Opt. Lett. 22 (13) (1997) 961–963.
[40] J. Knight, T. Birks, P.S.J. Russell, J. De Sandro, Properties of photonic crystal fiber and the effective index model, J. Opt. Soc. Amer. A 15 (3) (1998) 748–752.
[41] R. Cregan, B. Mangan, J. Knight, T. Birks, P.S.J. Russell, P. Roberts, D. Allan, Single-mode photonic band gap guidance of light in air, Science 285 (5433) (1999) 1537–1539.
[42] J.K. Ranka, R.S. Windeler, A.J. Stentz, Visible continuum generation in air–silica microstructure optical fibers with anomalous dispersion at 800 nm, Opt. Lett. 25 (1) (2000) 25–27.
[43] A. Ortigosa-Blanch, J. Knight, W. Wadsworth, J. Arriaga, B. Mangan, T. Birks, P.S.J. Russell, Highly birefringent photonic crystal fibers, Opt. Lett. 25 (18) (2000) 1325–1327.
[44] J. Knight, J. Arriaga, T. Birks, A. Ortigosa-Blanch, W. Wadsworth, P.S.J. Russell, Anomalous dispersion in photonic crystal fiber, IEEE Photonics Technol. Lett. 12 (7) (2000) 807–809.
[45] F. Benabid, J.C. Knight, G. Antonopoulos, P.S.J. Russell, Stimulated Raman scattering in hydrogen-filled hollow-core photonic crystal fiber, Science 298 (5592) (2002) 399–402.
[46] P. Russell, Photonic crystal fibers, Science 299 (5605) (2003) 358–362.
[47] J.G. Rarity, J. Fulconis, J. Duligall, W.J. Wadsworth, P.S.J. Russell, Photonic crystal fiber source of correlated photon pairs, Opt. Express 13 (2) (2005) 534–544.
[48] J.M. Dudley, G. Genty, S. Coen, Supercontinuum generation in photonic crystal fiber, Rev. Modern Phys. 78 (4) (2006) 1135.
[49] L. Rindorf, J.B. Jensen, M. Dufva, L.H. Pedersen, P.E. Høiby, O. Bang, Photonic crystal fiber long-period gratings for biochemical sensing, Opt. Express 14 (18) (2006) 8224–8231.
[50] D.K. Wu, B.T. Kuhlmey, B.J. Eggleton, Ultrasensitive photonic crystal fiber refractive index sensor, Opt. Lett. 34 (3) (2009) 322–324.
[51] M. Caldarola, V.A. Bettachini, A.A. Rieznik, P.G. König, M.E. Masip, D.F. Grosz, A.V. Bragas, High-speed tunable photonic crystal fiber-based femtosecond soliton source without dispersion pre-compensation, Pap. Phys. 4 (1) (2012) 1–3.
[52] R. Holzwarth, T. Udem, T.W. Hänsch, J. Knight, W. Wadsworth, P.S.J. Russell, Optical frequency synthesizer for precision spectroscopy, Phys. Rev. Lett. 85 (11) (2000) 2264.
[53] H. Kano, H.-o. Hamaguchi, Characterization of a supercontinuum generated from a photonic crystal fiber and its application to coherent Raman spectroscopy, Opt. Lett. 28 (23) (2003) 2360–2362.
[54] H. Kano, H.-o. Hamaguchi, Femtosecond coherent anti-Stokes Raman scattering spectroscopy using supercontinuum generated from a photonic crystal fiber, Appl. Phys. Lett. 85 (19) (2004) 4298–4300.
[55] H. Kano, H.-o. Hamaguchi, Ultrabroadband ($> 2500\,\mathrm{cm}^{-1}$) multiplex coherent anti-Stokes Raman scattering microspectroscopy using a supercontinuum generated from a photonic crystal fiber, Appl. Phys. Lett. 86 (12) (2005).
[56] H. Kano, H.-o. Hamaguchi, Vibrationally resonant imaging of a single living cell by supercontinuum-based multiplex coherent anti-Stokes Raman scattering microspectroscopy, Opt. Express 13 (4) (2005) 1322–1327.
[57] H. Kano, H.-o. Hamaguchi, Dispersion-compensated supercontinuum generation for ultrabroadband multiplex coherent anti-Stokes Raman scattering spectroscopy, J. Raman Spectrosc. 37 (1–3) (2006) 411–415.
[58] H. Kano, H.-o. Hamaguchi, In-vivo multi-nonlinear optical imaging of a living cell using a supercontinuum light source generated from a photonic crystal fiber, Opt. Express 14 (7) (2006) 2798–2804.
[59] H. Kano, H.-o. Hamaguchi, Supercontinuum dynamically visualizes a dividing single cell, Anal. Chem. 79 (23) (2007) 8967–8973.
[60] P. Li, K. Shi, Z. Liu, Manipulation and spectroscopy of a single particle by use of white-light optical tweezers, Opt. Lett. 30 (2) (2005) 156–158.
[61] B. von Vacano, W. Wohlleben, M. Motzkus, Actively shaped supercontinuum from a photonic crystal fiber for nonlinear coherent microspectroscopy, Opt. Lett. 31 (3) (2006) 413–415.
[62] J. Langridge, T. Laurila, R. Watt, R. Jones, C. Kaminski, J. Hult, Cavity enhanced absorption spectroscopy of multiple trace gas species using a supercontinuum radiation source, Opt. Express 16 (14) (2008) 10178–10188.

[63] M. Okuno, H. Kano, P. Leproux, V. Couderc, H.-o. Hamaguchi, Ultrabroadband multiplex CARS microspectroscopy and imaging using a subnanosecond supercontinuum light source in the deep near infrared, Opt. Lett. 33 (9) (2008) 923–925.
[64] H. Tu, S.A. Boppart, Coherent fiber supercontinuum for biophotonics, Laser Photonics Rev. 7 (5) (2013) 628–645.
[65] C. Dunsby, P.M.P. Lanigan, J. McGinty, D.S. Elson, J. Requejo-Isidro, I. Munro, N. Galletly, F. McCann, B. Treanor, B. Önfelt, D.M. Davis, M.A.A. Neil, P.M.W. French, An electronically tunable ultrafast laser source applied to fluorescence imaging and fluorescence lifetime imaging microscopy, J. Phys. D: Appl. Phys. 37 (23) (2004) 3296.
[66] J. Palero, V. Boer, J. Vijverberg, H. Gerritsen, H. Sterenborg, Short-wavelength two-photon excitation fluorescence microscopy of tryptophan with a photonic crystal fiber based light source, Opt. Express 13 (14) (2005) 5363–5368.
[67] E.R. Andresen, H.N. Paulsen, V. Birkedal, J. Thøgersen, S.R. Keiding, Broadband multiplex coherent anti-Stokes Raman scattering microscopy employing photonic-crystal fibers, J. Opt. Soc. Am. B 22 (9) (2005) 1934–1938.
[68] J. Frank, A. Elder, J. Swartling, A. Venkitaraman, A. Jeyasekharan, C. Kaminski, A white light confocal microscope for spectrally resolved multidimensional imaging, J. Microsc. 227 (Pt 3) (2007) 203–215.
[69] I. Hartl, X. Li, C. Chudoba, R. Ghanta, T. Ko, J. Fujimoto, J. Ranka, R. Windeler, Ultrahigh-resolution optical coherence tomography using continuum generation in an air–silica microstructure optical fiber, Opt. Lett. 26 (9) (2001) 608–610.
[70] W. Drexler, Ultrahigh-resolution optical coherence tomography, J. Biomed. Opt. 9 (1) (2004) 47–74.
[71] C. De Matos, S. Popov, J. Taylor, Temporal and noise characteristics of continuous-wave-pumped continuum generation in holey fibers around 1300nm, Appl. Phys. Lett. 85 (14) (2004) 2706–2708.
[72] P.-L. Hsiung, Y. Chen, T.H. Ko, J.G. Fujimoto, C.J. de Matos, S.V. Popov, J.R. Taylor, V.P. Gapontsev, Optical coherence tomography using a continuous-wave, high-power, Raman continuum light source, Opt. Express 12 (22) (2004) 5287–5295.
[73] A.D. Aguirre, N. Nishizawa, J.G. Fujimoto, W. Seitz, M. Lederer, D. Kopf, Continuum generation in a novel photonic crystal fiber for ultrahigh resolution optical coherence tomography at 800 nm and 1300 nm, Opt. Express 14 (3) (2006) 1145–1160.
[74] H. Wang, C.P. Fleming, A.M. Rollins, Ultrahigh-resolution optical coherence tomography at 1.15 μm using photonic crystal fiber with no zero-dispersion wavelengths, Opt. Express 15 (6) (2007) 3085–3092.
[75] T. Udem, R. Holzwarth, T.W. Hänsch, Optical frequency metrology, Nature 416 (6877) (2002) 233–237.
[76] J.T. Woodward, A.W. Smith, C.A. Jenkins, C. Lin, S.W. Brown, K.R. Lykke, Supercontinuum sources for metrology, Metrologia 46 (4) (2009) S277.
[77] B. Kibler, J. Dudley, S. Coen, Supercontinuum generation and nonlinear pulse propagation in photonic crystal fiber: Influence of the frequency-dependent effective mode area, Appl. Phys. B 81 (2005) 337–342.
[78] R. Driben, A. Husakou, J. Herrmann, Low-threshold supercontinuum generation in glasses doped with silver nanoparticles, Opt. Express 17 (20) (2009) 17989–17995.
[79] F. Arteaga-Sierra, A. Antikainen, G.P. Agrawal, Soliton dynamics in photonic-crystal fibers with frequency-dependent Kerr nonlinearity, Phys. Rev. A 98 (1) (2018) 013830.
[80] R. Driben, J. Herrmann, Solitary pulse propagation and soliton-induced supercontinuum generation in silica glasses containing silver nanoparticles, Opt. Lett. 35 (15) (2010) 2529–2531.
[81] S. Zhao, X. Sun, Soliton dynamics in an all-normal-dispersion photonic crystal fiber with frequency-dependent Kerr nonlinearity, Phys. Rev. A 102 (3) (2020) 033514.
[82] S. Bose, R. Chattopadhyay, S. Roy, S.K. Bhadra, Study of nonlinear dynamics in silver-nanoparticle-doped photonic crystal fiber, J. Opt. Soc. Am. B 33 (6) (2016) 1014–1021.
[83] S. Bose, A. Sahoo, R. Chattopadhyay, S. Roy, S.K. Bhadra, G.P. Agrawal, Implications of a zero-nonlinearity wavelength in photonic crystal fibers doped with silver nanoparticles, Phys. Rev. A 94 (4) (2016) 043835.
[84] S. Bose, R. Chattopadhyay, M. Pal, S. Bhadra, Effect of zero-nonlinearity point on optical event horizon in defocused nonlinear media, in: 2017 XXXIInd General Assembly and Scientific Symposium of the International Union of Radio Science, URSI GASS, IEEE, 2017, pp. 1–3.
[85] S. Bose, G. Steinmeyer, U. Morgner, A. Demircan, Controlling the temporal trajectory of solitons in silver nanoparticle doped fibre, in: 2019 Conference on Lasers and Electro-Optics Europe & European Quantum Electronics Conference, CLEO/Europe-EQEC, IEEE, 2019, p. 1.
[86] S. Bose, O. Melchert, S. Willms, I. Babushkin, U. Morgner, A. Demircan, G.P. Agrawal, Role of frequency dependence of the nonlinearity on a soliton's evolution in photonic crystal fibers, Opt. Lett. 46 (16) (2021) 3921–3924.
[87] F.R. Arteaga-Sierra, A. Antikainen, G.P. Agrawal, Soliton mitosis across a zero-nonlinearity wavelength in photonic crystal fibers, Front. Opt. 2017 (2017) FTu5A.2.
[88] F.R. Arteaga-Sierra, A. Antikainen, G.P. Agrawal, Raman-shift suppression and soliton splitting in photonic crystal fibers with nonlinear dispersion, in: Conference on Lasers and Electro-Optics, Optica Publishing Group, 2017, p. JTu5A.62.
[89] O. Melchert, S. Bose, S. Willms, I. Babushkin, U. Morgner, A. Demircan, Two-color pulse compounds in waveguides with a zero-nonlinearity point, Opt. Lett. 48 (2) (2023) 518–521.
[90] K.J. Blow, D. Wood, Theoretical description of transient stimulated Raman scattering in optical fibers, IEEE J. Quantum Electron. 25 (12) (1989) 2665–2673.
[91] P. Mamyshev, S.V. Chernikov, Ultrashort-pulse propagation in optical fibers, Opt. Lett. 15 (19) (1990) 1076–1078.
[92] N. Karasawa, S. Nakamura, N. Nakagawa, M. Shibata, R. Morita, H. Shigekawa, M. Yamashita, Comparison between theory and experiment of nonlinear propagation for a-few-cycle and ultrabroadband optical pulses in a fused-silica fiber, IEEE J. Quantum Electron. 37 (3) (2001) 398–404.
[93] R. Stolen, E. Ippen, Raman gain in glass optical waveguides, Appl. Phys. Lett. 22 (6) (1973) 276–278.
[94] R.H. Stolen, J.P. Gordon, W. Tomlinson, H.A. Haus, Raman response function of silica-core fibers, J. Opt. Soc. Am. B 6 (6) (1989) 1159–1166.
[95] M.N. Islam, Raman amplifiers for telecommunications, IEEE J. Sel. Top. Quantum Electron. 8 (3) (2002) 548–559.
[96] K. Blow, D. Wood, Theoretical description of transient stimulated Raman scattering in optical fibers, IEEE J. Quantum Electron. 25 (12) (1989) 2665–2673, http://dx.doi.org/10.1109/3.40655.
[97] R.W. Boyd, Nonlinear Optics, Academic Press, 2008.
[98] J. Bonetti, N. Linale, A.D. Sánchez, S.M. Hernandez, P.I. Fierens, D.F. Grosz, Modified nonlinear Schrödinger equation for frequency-dependent nonlinear profiles of arbitrary sign, J. Opt. Soc. Am. B 36 (11) (2019) 3139–3144.
[99] J. Bonetti, N. Linale, A.D. Sánchez, S.M. Hernández, P.I. Fierens, D.F. Grosz, Photon-conserving generalized nonlinear Schrödinger equation for frequency-dependent nonlinearities, J. Opt. Soc. Am. B 37 (2) (2020) 445–450.
[100] N. Linale, P.I. Fierens, D.F. Grosz, Revisiting soliton dynamics in fiber optics under strict photon-number conservation, IEEE J. Quantum Electron. 57 (2) (2020) 1–8.
[101] N. Linale, P.I. Fierens, J. Bonetti, A.D. Sánchez, S.M. Hernandez, D.F. Grosz, Measuring self-steepening with the photon-conserving nonlinear Schrödinger equation, Opt. Lett. 45 (16) (2020) 4535–4538.
[102] S.M. Hernández, J. Bonetti, N. Linale, D.F. Grosz, P.I. Fierens, Soliton solutions and self-steepening in the photon-conserving nonlinear Schrödinger equation, Waves Random Complex Media (2020) 1–17.
[103] N. Linale, J. Bonetti, A.D. Sánchez, S.M. Hernandez, P.I. Fierens, D.F. Grosz, Modulation instability in waveguides with an arbitrary frequency-dependent nonlinear coefficient, Opt. Lett. 45 (9) (2020) 2498–2501.

[104] N. Vermeulen, D. Castelló-Lurbe, J. Cheng, I. Pasternak, A. Krajewska, T. Ciuk, W. Strupinski, H. Thienpont, J. Van Erps, Negative Kerr nonlinearity of graphene as seen via chirped-pulse-pumped self-phase modulation, Phys. Rev. Appl. 6 (4) (2016) 044006.
[105] A. Ishizawa, R. Kou, T. Goto, T. Tsuchizawa, N. Matsuda, K. Hitachi, T. Nishikawa, K. Yamada, T. Sogawa, H. Gotoh, Optical nonlinearity enhancement with graphene-decorated silicon waveguides, Sci. Rep. 7 (1) (2017) 45520.
[106] N. Linale, J. Bonetti, A.D. Sánchez, P.I. Fierens, D.F. Grosz, Model for frequency-dependent nonlinear propagation in 2D-decorated nanowires, IEEE J. Quantum Electron. 57 (4) (2021) 1–8.
[107] N. Linale, P.I. Fierens, N. Vermeulen, D.F. Grosz, A generic model for the study of supercontinuum generation in graphene-covered nanowires, J. Phys.: Photon. 4 (1) (2021) 015001.
[108] P.I. Fierens, S.M. Hernandez, N. Linale, D.F. Grosz, Theoretical analysis of spectral broadening through saturable photoexcited-carrier refraction in graphene-covered nanowires, IEEE J. Quantum Electron. 58 (6) (2022) 1–5.
[109] Y.-R. Shen, Principles of nonlinear optics, Wiley-Interscience, New York, NY, USA, 1984.
[110] A. Ferrando, M. Zacarés, P.F. de Córdoba, D. Binosi, Á. Montero, Forward-backward equations for nonlinear propagation in axially invariant optical systems, Phys. Rev. E 71 (1) (2005) 016601.
[111] M. Kolesik, J. Moloney, M. Mlejnek, Unidirectional optical pulse propagation equation, Phys. Rev. Lett. 89 (28) (2002) 283902.
[112] T. Brabec, F. Krausz, Nonlinear optical pulse propagation in the single-cycle regime, Phys. Rev. Lett. 78 (17) (1997) 3282.
[113] M.A. Porras, Propagation of single-cycle pulsed light beams in dispersive media, Phys. Rev. A 60 (6) (1999) 5069.
[114] P. Kinsler, G. New, Few-cycle pulse propagation, Phys. Rev. A 67 (2) (2003) 023813.
[115] P. Kinsler, G. New, Few-cycle soliton propagation, Phys. Rev. A 69 (1) (2004) 013805.
[116] S. Iz'' yurov, S. Kozlov, Dynamics of the spatial spectrum of a self-focusing optical wave in a nonlinear medium, J. Exp. Theoret. Phys. Lett. 71 (2000) 453–456.
[117] V. Bespalov, S. Kozlov, Y.A. Shpolyanskiy, I. Walmsley, Simplified field wave equations for the nonlinear propagation of extremely short light pulses, Phys. Rev. A 66 (1) (2002) 013811.
[118] A. Husakou, J. Herrmann, Supercontinuum generation of higher-order solitons by fission in photonic crystal fibers, Phys. Rev. Lett. 87 (20) (2001) 203901.
[119] M. Kolesik, J.V. Moloney, Nonlinear optical pulse propagation simulation: From Maxwell's to unidirectional equations, Phys. Rev. E 70 (3) (2004) 036604.
[120] G. Genty, P. Kinsler, B. Kibler, J. Dudley, Nonlinear envelope equation modeling of sub-cycle dynamics and harmonic generation in nonlinear waveguides, Opt. Express 15 (9) (2007) 5382–5387.
[121] Y. Mizuta, M. Nagasawa, M. Ohtani, M. Yamashita, Nonlinear propagation analysis of few-optical-cycle pulses for subfemtosecond compression and carrier envelope phase effect, Phys. Rev. A 72 (6) (2005) 063802.
[122] P. Kinsler, S. Radnor, G. New, Theory of directional pulse propagation, Phys. Rev. A 72 (6) (2005) 063807.
[123] P. Kinsler, Limits of the unidirectional pulse propagation approximation, J. Opt. Soc. Am. B 24 (9) (2007) 2363–2368.
[124] P. Kinsler, Optical pulse propagation with minimal approximations, Phys. Rev. A 81 (1) (2010) 013819.
[125] S. Amiranashvili, A. Demircan, Hamiltonian structure of propagation equations for ultrashort optical pulses, Phys. Rev. A 82 (1) (2010) 013812.
[126] S. Amiranashvili, A. Demircan, Ultrashort optical pulse propagation in terms of analytic signal, Adv. Opt. Technol. 2011 (2011).
[127] S. Amiranashvili, U. Bandelow, N. Akhmediev, Few-cycle optical solitary waves in nonlinear dispersive media, Phys. Rev. A 87 (1) (2013) 013805.
[128] S. Amiranashvili, Hamiltonian framework for short optical pulses, in: E. Tobisch (Ed.), New Approaches to Nonlinear Waves, Springer International Publishing, Cham, 2016, pp. 153–196.
[129] S. Amiranashvili, M. Radziunas, U. Bandelow, R. Čiegis, Numerical methods for accurate description of ultrashort pulses in optical fibers, Commun. Nonlinear Sci. Numer. Simul. 67 (2019) 391–402.
[130] L. Pitaevskii, S. Stringari, Bose-Einstein Condensation and Superfluidity, vol. 164, Oxford University Press, 2003.
[131] N.K. Efremidis, J. Hudock, D.N. Christodoulides, J.W. Fleischer, O. Cohen, M. Segev, Two-dimensional optical lattice solitons, Phys. Rev. Lett. 91 (21) (2003) 213906.
[132] S.-S. Yu, C.-H. Chien, Y. Lai, J. Wang, Spatio-temporal solitary pulses in graded-index materials with Kerr nonlinearity, Opt. Commun. 119 (1–2) (1995) 167–170.
[133] S. Raghavan, G.P. Agrawal, Spatiotemporal solitons in inhomogeneous nonlinear media, Opt. Commun. 180 (4–6) (2000) 377–382.
[134] W.H. Renninger, F.W. Wise, Optical solitons in graded-index multimode fibres, Nature Commun. 4 (1) (2013) 1719.
[135] R. Hellwarth, Third-order optical susceptibilities of liquids and solids, Prog. Quantum Electron. 5 (1977) 1–68.
[136] N. Tang, R. Sutherland, Time-domain theory for pump–probe experiments with chirped pulses, J. Opt. Soc. Am. B 14 (12) (1997) 3412–3423.
[137] A. Martınez-Rios, A.N. Starodumov, Y.O. Barmenkov, V. Filippov, I. Torres-Gomez, Influence of the symmetry rules for Raman susceptibility on the accuracy of nonlinear index measurements in optical fibers, J. Opt. Soc. Am. B 18 (6) (2001) 794–803.
[138] D. Milam, Review and assessment of measured values of the nonlinear refractive-index coefficient of fused silica, Appl. Opt. 37 (3) (1998) 546–550.
[139] J.J. Garcıa-Ripoll, V.V. Konotop, B. Malomed, V.M. Pérez-Garcıa, A quasi-local Gross–Pitaevskii equation for attractive Bose–Einstein condensates, Math. Comput. Simulation 62 (1–2) (2003) 21–30.
[140] N.C. Panoiu, X. Liu, R.M. Osgood, Nonlinear dispersion in silicon photonic wires, in: 2008 Conference on Lasers and Electro-Optics and 2008 Conference on Quantum Electronics and Laser Science, IEEE, 2008, pp. 1–2.
[141] N.C. Panoiu, X. Liu, R.M. Osgood Jr., Self-steepening of ultrashort pulses in silicon photonic nanowires, Opt. Lett. 34 (7) (2009) 947–949.
[142] J. Lægsgaard, Mode profile dispersion in the generalized nonlinear Schrödinger equation, Opt. Express 15 (24) (2007) 16110–16123.
[143] J. Lægsgaard, P.J. Roberts, Dispersive pulse compression in hollow-core photonic bandgap fibers, Opt. Express 16 (13) (2008) 9628–9644.
[144] O. Vanvincq, J.C. Travers, A. Kudlinski, Conservation of the photon number in the generalized nonlinear Schrödinger equation in axially varying optical fibers, Phys. Rev. A 84 (6) (2011) 063820.
[145] J. Lægsgaard, Modeling of nonlinear propagation in fiber tapers, J. Opt. Soc. Am. B 29 (11) (2012) 3183–3191.
[146] M. Kolesik, E.M. Wright, J.V. Moloney, Simulation of femtosecond pulse propagation in sub-micron diameter tapered fibers, Appl. Phys. B 79 (2004) 293–300.
[147] R.C. Miller, Optical second harmonic generation in piezoelectric crystals, Appl. Phys. Lett. 5 (1) (1964) 17–19.
[148] M. Bell, Frequency dependence of Miller's rule for nonlinear susceptibilities, Phys. Rev. B 6 (2) (1972) 516.
[149] Y. Lai, H. Haus, Quantum theory of solitons in optical fibers. I. Time-dependent Hartree approximation, Phys. Rev. A 40 (2) (1989) 844.
[150] J. Bonetti, A. Sánchez, S. Hernandez, D. Grosz, A simple approach to the quantum theory of nonlinear fiber optics, 2019, arXiv preprint arXiv:1902.00561.
[151] J. Bonetti, S.M. Hernandez, D.F. Grosz, Master equation approach to propagation in nonlinear fibers, Opt. Lett. 46 (3) (2021) 665–668.
[152] P. Pearle, Simple derivation of the Lindblad equation, Eur. J. Phys. 33 (4) (2012) 805.
[153] N. Linale, J. Bonetti, A. Sparapani, A.D. Sánchez, D.F. Grosz, Equation for modeling two-photon absorption in nonlinear waveguides, J. Opt. Soc. Am. B 37 (6) (2020) 1906–1910.
[154] J. Hult, A fourth-order Runge–Kutta in the interaction picture method for simulating supercontinuum generation in optical fibers, J. Lightwave Technol. 25 (12) (2007) 3770–3775.
[155] G. Kuracz, L.R. Kiperman, F. Reyna, P.I. Fierens, Simulation of pulse propagation in nonlinear optical fibers using GPUs, in: IEEE CACIDI 2016-IEEE Conference on Computer Sciences, IEEE, 2016, pp. 1–5.

[156] N. Linale, P.I. Fierens, S.M. Hernandez, J. Bonetti, D.F. Grosz, Narrowband and ultra-wideband modulation instability in nonlinear metamaterial waveguides, J. Opt. Soc. Am. B 37 (11) (2020) 3194–3199.
[157] P. Shukla, J.J. Rasmussen, Modulational instability of short pulses in long optical fibers, Opt. Lett. 11 (3) (1986) 171–173.
[158] C. De Angelis, G. Nalesso, M. Santagiustina, Role of nonlinear dispersion in the dynamics of induced modulational instability in Kerr media, J. Opt. Soc. Am. B 13 (5) (1996) 848–855.
[159] S.M. Hernandez, P.I. Fierens, J. Bonetti, A.D. Sánchez, D.F. Grosz, A geometrical view of scalar modulation instability in optical fibers, IEEE Photonics J. 9 (5) (2017) 1–8.
[160] A. Zheltikov, Optical shock wave and photon-number conservation, Phys. Rev. A 98 (4) (2018) 043833.
[161] D. Marcuse, RMS width of pulses in nonlinear dispersive fibers, J. Lightwave Technol. 10 (1) (1992) 17–21.
[162] J. Santhanam, G.P. Agrawal, Raman-induced spectral shifts in optical fibers: General theory based on the moment method, Opt. Commun. 222 (1–6) (2003) 413–420.
[163] Z. Chen, A.J. Taylor, A. Efimov, Soliton dynamics in non-uniform fiber tapers: Analytical description through an improved moment method, J. Opt. Soc. Am. B 27 (5) (2010) 1022–1030.
[164] N. Linale, J. Bonetti, P.I. Fierens, S.M. Hernandez, D.F. Grosz, A direct method for the simultaneous estimation of self-steepening and the fractional Raman contribution in fiber optics, IEEE J. Quantum Electron. 57 (3) (2021) 1–7.
[165] S. Zhao, R. Guo, Y. Zeng, Effects of frequency-dependent Kerr nonlinearity on higher-order soliton evolution in a photonic crystal fiber with one zero-dispersion wavelength, Phys. Rev. A 106 (3) (2022) 033516.
[166] S. Hernandez, A. Sparapani, N. Linale, J. Bonetti, D. Grosz, P. Fierens, Dispersive waves and radiation trapping in optical fibers with a zero-nonlinearity wavelength, Waves Random Complex Media (2022) 1–15.
[167] A. Sparapani, J. Bonetti, N. Linale, S. Hernandez, P. Fierens, D. Grosz, Temporal reflection and refraction in the presence of a zero-nonlinearity wavelength, Opt. Lett. 48 (2) (2023) 339–342.
[168] A. Sparapani, G. Fernández, A. Sánchez, J. Bonetti, N. Linale, D. Grosz, All-optical pulse-train generation through the temporal analogue of a laser, Opt. Fiber Technol., Mater. Devices Syst. 68 (2022) 102785.
[169] O. Melchert, C. Brée, A. Tajalli, A. Pape, R. Arkhipov, S. Willms, I. Babushkin, D. Skryabin, G. Steinmeyer, U. Morgner, et al., All-optical supercontinuum switching, Commun. Phys. 3 (1) (2020) 1–8.
[170] A.C. Sparapani, L.N. Gutierrez, S.M. Hernandez, P.I. Fierens, D.F. Grosz, G.P. Agrawal, Raman suppression and all-optical control in media with a zero-nonlinearity wavelength, IEEE J. Quantum Electron. (2024) 1–1.